A Generalized Base-Flow Analysis with Initial Boundary-Layer and Chemistry Effects

John H. Fox
ARO, Inc.

July 1979

Final Report for Period October 1, 1976 – May 18, 1979

Approved for public release; distribution unlimited.

ARNOLD ENGINEERING DEVELOPMENT CENTER
ARNOLD AIR FORCE STATION, TENNESSEE
AIR FORCE SYSTEMS COMMAND
UNITED STATES AIR FORCE

NOTICES

When U. S. Government drawings, specifications, or other data are used for any purpose other than a definitely related Government procurement operation, the Government thereby incurs no responsibility nor any obligation whatsoever, and the fact that the Government may have formulated, furnished, or in any way supplied the said drawings, specifications, or other data, is not to be regarded by implication or otherwise, or in any manner licensing the holder or any other person or corporation, or conveying any rights or permission to manufacture, use, or sell any patented invention that may in any way be related thereto.

Qualified users may obtain copies of this report from the Defense Documentation Center.

References to named commerical products in this report are not to be considered in any sense as an indorsement of the product by the United States Air Force or the Government.

This report has been reviewed by the Information Office (OI) and is releasable to the National Technical Information Service (NTIS). At NTIS, it will be available to the general public, including foreign nations.

APPROVAL STATEMENT

This report has been reviewed and approved.

Elton R. Thompson

ELTON R. THOMPSON
Project Manager, Research Division
Directorate of Test Engineering

Approved for publication:

FOR THE COMMANDER

Robert W. Crossley

ROBERT W. CROSSLEY, Lt Colonel, USAF
Acting Director of Test Engineering
Deputy for Operations

REPORT DOCUMENTATION PAGE		READ INSTRUCTIONS BEFORE COMPLETING FORM
1. REPORT NUMBER AEDC-TR-79-46	2. GOVT ACCESSION NO.	3. RECIPIENT'S CATALOG NUMBER
4. TITLE (and Subtitle) A GENERALIZED BASE-FLOW ANALYSIS WITH INITIAL BOUNDARY-LAYER AND CHEMISTRY EFFECTS		5. TYPE OF REPORT & PERIOD COVERED Final Report - Oct 1, 1976 - May 18, 1979 6. PERFORMING ORG. REPORT NUMBER
7. AUTHOR(s) John H. Fox, ARO, Inc., a Sverdrup Corporation Company		8. CONTRACT OR GRANT NUMBER(s)
9. PERFORMING ORGANIZATION NAME AND ADDRESS Arnold Engineering Development Center/DOTR Air Force Systems Command Arnold Air Force Station, TN 37389		10. PROGRAM ELEMENT, PROJECT, TASK AREA & WORK UNIT NUMBERS Program Element 65807F
11. CONTROLLING OFFICE NAME AND ADDRESS Arnold Engineering Development Center/OIS Air Force Systems Command Arnold Air Force Station, TN 37389		12. REPORT DATE July 1979 13. NUMBER OF PAGES 116
14. MONITORING AGENCY NAME & ADDRESS(if different from Controlling Office)		15. SECURITY CLASS. (of this report) UNCLASSIFIED 15a. DECLASSIFICATION/DOWNGRADING SCHEDULE N/A

16. DISTRIBUTION STATEMENT (of this Report)

Approved for public release; distribution unlimited.

17. DISTRIBUTION STATEMENT (of the abstract entered in Block 20, if different from Report)

18. SUPPLEMENTARY NOTES

Available in DDC

19. KEY WORDS (Continue on reverse side if necessary and identify by block number)

supersonic flow	chemical eqiuilibrium
mixing	enthalpy
theory	axisymmetric
jet mixing flow	bodies
boundary layer	base flow

20. ABSTRACT (Continue on reverse side if necessary and identify by block number)

A general theory has been developed for the supersonic, turbulent, near-wake region behind bluff-based, two-dimensional and axially symmetric bodies in the presence of a coaxial, supersonic jet. This work is a generalization of the theory of H. H. Korst and his co-workers. The present theory includes the effects of the initial boundary layer, base bleed, total enthalpy and species differences, and equilibrium chemistry. The generalization was accomplished

DD FORM 1 JAN 73 1473 EDITION OF 1 NOV 65 IS OBSOLETE

20. ABSTRACT (Continued)

through the development of an analytical recompression model that obviates the requirement for a recompression factor; the development of a species distribution model for the mixing layers; and the use of a new spreading parameter for the axially symmetric problem. The theory shows good agreement with experiment for the classical, planar-backstep problem with both thin and very thick boundary layers. Good agreement is also shown with base flows behind axially symmetric bodies with a coaxial jet.

AFSC
Arnold AFS Tenn

PREFACE

The work reported herein was conducted by the Arnold Engineering Development Center (AEDC), Air Force Systems Command (AFSC). The Air Force project manager was Elton R. Thompson, DOTR. The results of the research were obtained by ARO, Inc., AEDC Division (a Sverdrup Corporation Company), operating contractor for the AEDC, AFSC, Arnold Air Force Station, Tennessee, under ARO Project Number F32Y-03A. The manuscript was submitted for publication on May 18, 1979.

This material was also submitted as a dissertation in partial fulfillment of the requirements for the degree of Doctor of Philosophy, The University of Tennessee, Knoxville, Tennessee, in March 1979.

The author wishes to acknowledge Mr. Robert C. Bauer, ARO, Inc., for his role in this work. He served as teacher, critic, and co-worker. His day-to-day technical advice, continued encouragement, and good humor served to make the task at once good fun and intellectually rewarding. Special thanks also must go to Dr. Jain-Ming Wu, The University of Tennessee Space Institute, Tullahoma, Tennessee, for his interest in the work and the necessary prodding he provided. Other ARO co-workers who provided technical advice were Messrs. K. R. Kneile, C. E. Peters, and F. C. Loper.

TABLE OF CONTENTS

LIST OF FIGURES

CHAPTER I

INTRODUCTION

I. Purpose

Perhaps the most common configuration of vehicles capable of supersonic flight is that of a supersonic nozzle embedded in a blunt-based afterbody, as typified in Fig. 1. The complex flow interactions occurring as the outer stream and nozzle exhaust expand into the lower pressure of the base, mix with the base gas, and recompress to the downstream pressure are not well understood. However, it is of importance to the designer to know the properties of the mixture of the low-velocity gases recirculated into the base region as they are at a pressure lower than the ambient stream, and they contribute significantly to the drag of the vehicle. Thus, a detailed knowledge of how the base pressure and temperature are affected by the boundary layer buildup on the outer surface of the afterbody, by the flare angle of the nozzle, by the constituents of the nozzle gas, and by the injection of various gases into the base is required in order to optimize a design. Those interested in the structure of rocket plumes are concerned with the effect base properties have on the Mach disk location and the destruction of the coherent inviscid plume. And, of course, the engineer in planning a test

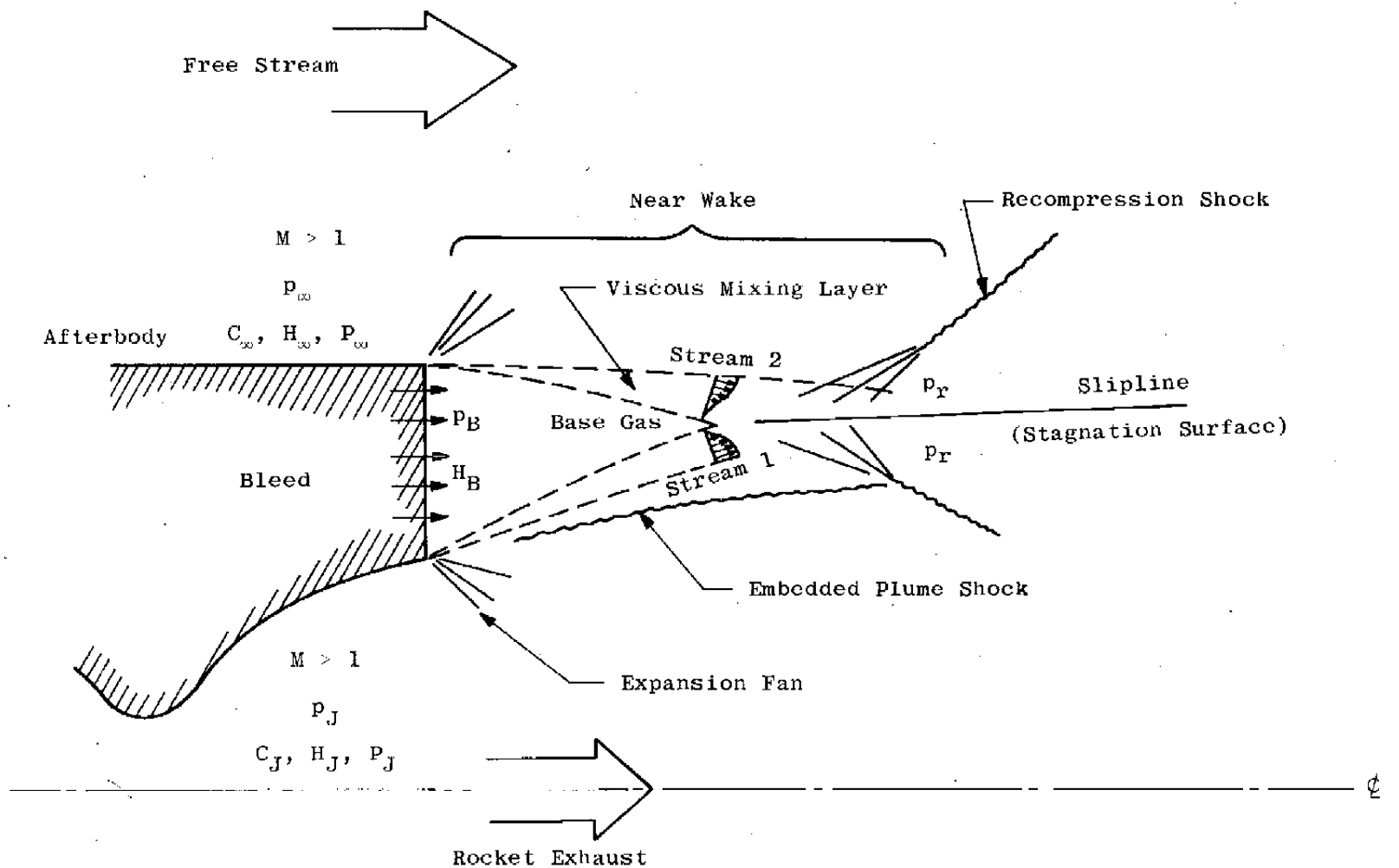

Figure 1. General plume-stream interaction.

configuration must have some indication of what to expect from a given vehicle design at various simulated flight conditions, a method of confirming anomalies in his data, and the knowledge to interpret and extend the usefulness of his data.

It is the purpose, then, of this investigation to present a new theoretical model capable of predicting the base properties behind blunt-based bodies with supersonic nozzles at supersonic speed taking into account the boundary layer existing at separation, base bleed, and chemistry. This study, however, must be considered a progress report since, as is always the case, limitations of time and resources have left several avenues of investigation underdeveloped.

Although this work is new and comprehensive, it makes use of well-established principles first presented by H. H. Korst and his co-workers [1][1] and extended by Bauer and Fox [2]. Thus, it is perhaps appropriate to focus on the primary departures from earlier concepts.

One of the primary obstacles to a comprehensive base-flow theory is the recompression process. If the classical planar, backward-facing step is considered, for example, the recompression process serves to compress the high-speed gas in the mixing layer, from what is

[1]Numbers in brackets refer to similarly numbered references in the Bibliography.

essentially the pressure existing within the base region, to the free-stream pressure. If the flow were inviscid, the pressure would be adjusted abruptly by an inviscid shock. However, experiments show that viscous effects stretch out the process significantly. The streamline dividing that part of the mixing layer which experiences recompression from that part which turns back toward the base must be identified in order for the theory to have closure. It is identified by the pressure to which it stagnates. As this pressure is unknown, earlier workers made up empirically determined recompression factors to provide the required information. In the present work, a hypothesis is put forward which serves to couple the momentum of the oncoming, viscous layer to the observed recompression profile of the pressure on the downstream wall. This hypothesis is a fundamental refinement to the geometrical recompression theory of Bauer and Fox [2].

When considering base bleed or the general problem of the mixing of disparate streams into the base region, the distribution of the species through the mixing zone presents difficulties for existing theories when the initial boundary layer is taken into account. The usual procedure is to consider the species profile to be identical to the velocity profile. To understand that this is incorrect, one needs only to consider that at the point of separation the species profile is that of a step function while the velocity profile is that of the initial

boundary layer. Consequently, in the present theory, a new profile for the species distribution is proposed which serves to account appropriately for this distinction. This profile nicely approaches the velocity profile in the limit of fully developed flow.

When extending the theory to axially symmetric flows, the mixing theory must be modified. An analysis is presented in this work which demonstrates that the Mangler transformation serves to confirm the mixing theory of Bauer and Fox [2].

And finally, since the mechanisms were developed with the overall theory, it was a relatively simple matter to incorporate equilibrium chemistry into the analysis. Thus the use of the so-called flame-sheet model is avoided.

Although the present work considers only turbulent flow, the extension to laminar flow is straightforward. The principal change would be in the analysis of the spreading parameter.

II. Primary Analytical Models

Even with the advent of the new generation of advanced computers, attacking such formidable problems as base flow with bleed and chemical effects by numerically solving the Navier-Stokes equations coupled with equilibrium chemistry is beyond present capabilities. Consequently, the approach has been and will continue to be that analagous to the boundary-layer problem; that is, to solve

the viscid and inviscid areas by different methods and to couple the solutions using the physical constraints at the interfaces.

There are two primary mixing theories extant that may be used in the base-flow problem: the Crocco-Lees [3] theory and the component model of Korst, et al. [1]. The Crocco-Lees theory and the Korst theory are similar only in one aspect: they both account for the strong viscous interactions that prevail in flows with mixing.

Crocco-Lees Model

The basic boundary-layer equations are integrated across the mixing layer. There results a set of integro-differential equations which are ordinary in the axial direction. The equations are linear with respect to the derivatives at any axial station. Thus, with the edge conditions known and the transverse profiles given, the mixing layer is calculated in a marching fashion by solving the inviscid field simultaneously to provide the edge conditions. Thus, the axial pressure gradients are part of the solution. In the flow of a single stream over a bluff-based body, the elliptic nature of the base flow is exhibited in an interesting fashion: if the guess of the initial base pressure is incorrect, the determinant of the derivatives goes to zero at some point in the recompression region. By properly adjusting the base pressure, the marching of the solution is made to proceed smoothly

through this point with the determinant of the augmented matrix going to zero simultaneously with that of the coefficient matrix. The method is physically realistic and includes the details of the actual flow.

The main drawbacks to this method which foreclose its use in the present analysis are twofold. Of first consideration is the complexity and difficulty of implementation of the method in any but the simplest of problems; it is not clear, for example, when there are two supersonic streams involving two converging mixing layers as well as a bleed flow, just how the base pressure is determined. Two separate singularities would have to be coupled and resolved requiring, at least, a detailed analysis of the reversed flow, such analysis making the Navier-Stokes approach a delight by comparison. Secondly, and equally important, is the finding by Peters and Phares [4] that the method breaks down when the species concentration equation is coupled into the system: anomalous singularities occur. (The problem apparently can be overcome by uncoupling the species equation from the system by appropriate modeling.) These concerns make the Crocco-Lees approach unattractive at this stage of its development.

Korst Mixing and Base-Flow Models

The basic Korst theory is so uncomplicated that for simple, fully developed, two-dimensional base flows the computations required can be performed on a desk calculator.

The basic simplicity of the mixing theory along with the good correlations that result from its use have made it one of the most widely adopted approaches to turbulent mixing problems [5]. A recent example of its use, essentially unmodified, is afforded by the work of Yaros [6], who used it to account for mixing between two coaxial streams. His results agreed well with observation.

The elemental Korst base-flow theory is made up of three distinct analyses:

1. Inviscid analysis to determine the overall flow structure and pressure field, sometimes referred to as the "corresponding" inviscid flow.
2. Global analysis of the assumed flow behavior in the near wake leading to the primary system of conservation equations for the base properties.
3. Viscous mixing and recompression analysis to determine key streamlines in the mixing region.

The simplicity is achieved through the assumption of isobaric mixing. This allows the mixing region to be completely determined at any point along the inviscid boundary as a function of the mixing pressure and the distance from inception. Thus the mixing analysis is uncoupled from the inviscid computations. The velocity profile is determined by simplification of the boundary-layer momentum equation to a heat conduction form that has

an error function solution. The only coupling to the inviscid flow is achieved by positioning the layer with respect to the inviscid boundary by a momentum balance.

For the simple, two-dimensional, base-pressure problem (flow over a backward-facing step), the Korst theory assumes that the dividing streamline, which discriminates between that part of the flow which goes through recompression and that which recirculates in the base region, isentropically stagnates to a pressure equal to the recompressed pressure. This knowledge allows a global mass conservation equation for the recirculating flow to be evaluated. The pressure is adjusted until a dividing streamline is determined that allows the global mass balance equation to be satisfied. At first glance, this appears to be an oversimplification of the problem; however, it models the major elements of the flow and correlates well with experiment.

Further investigation led to the conclusion that the remodeling of elements of the method would make it more general and thus applicable to the complex flows under consideration. Therefore, the Korst mixing and base-pressure theory, as developed and extended in the following chapters, is the method of choice.

III. Other Approaches

Over the years, the Korst and Crocco-Lees theories have stimulated similar approaches in an effort to find better agreement with observation. Several are reviewed.

Chow's Method

Chow [7] developed a base-pressure theory which uses the Korst constant-pressure mixing up to the point where recompression begins; whereupon, the mixing layer is split at the dividing streamline, the outer part exposed to a pressure gradient. The high-speed layer goes through recompression, while the low-speed layer is obverted and assumed to recirculate. The shear force along the dividing streamline must be equal at once to the gradient of the momentums in each layer. By modeling the shear stress, the gradients are known, and an integration in the direction of principal flow can be performed stepwise to the stagnation point, where the velocity of the dividing streamline is set to zero and the pressures assume particular values derived from momentum considerations on the stagnation surface. By assuming a base pressure and the distance from separation at which the recompression begins, the integration is able to proceed to stagnation where the dependent variables must match the boundary conditions on the stagnation surface. If they do not, a new guess of pressure and length is made and an iteration ensues until the integration predicts conditions at stagnation.

This analysis, while containing very realistic assumptions, is fairly complex and gives only fair predictions for thin boundary layers and poor results for very thick boundary layers.

Chow and Spring's Modification

This theory [8] is essentially a modification of the preceding theory. The constant-pressure mixing up to the onset of recompression is replaced with a refinement which includes a streamtube expansion of the initial boundary layer at the corner separation point. A linear velocity profile is then assumed that has the slope of an error-function profile at its half-velocity point. The method of solution is quite similar to the previous theory. The predictions of the theory are quite good for thicker boundary layers; however, here again the method is quite cumbersome.

Tanner's Method

Tanner's [9] approach is more analogous to the Korst theory than any other and is therefore attractive in its simplicity. His principal assumption is that the production of entropy of the recompression shock in an inviscid flow is identical to the entropy production when the reattached shear layer displaces the shock. That is, the lost entropy production of the displaced shock is made up by the entropy production of the shear layer. Tanner determines empirically the ratio of the distance from the

displaced inviscid shock and the thickness of the recompressing shear layer. He also assumes the velocity at the stagnation surface after the flow has reaccelerated. Base pressures are guessed in an iterative fashion until the condition of entropy equality is satisfied. Although Tanner does not take into account the initial boundary layer, his agreement with his own data is quite good; in fact, the theory of this investigation agrees with that of Tanner for a particular boundary-layer momentum thickness (see Chapter IV, Section II). The principal objection, however, is that it is not clear just how bleed flow could be incorporated into the theory, as Tanner does not employ any mass-rate accounting.

Extensions of the Basic Korst Model

Nash [10], Addy [11], and Page, et al. [12] are examples of the second generation of Korst theorists. They all resort to an empirically determined recompression factor to make their solutions agree with various data. Thus, as Peters and Phares [4] point out, ". . . these models really are used to correlate experimental base-pressure measurements rather than to predict them," as no universal factor has been developed.

Refinements of the Crocco-Lees Approach

The works of Peters and Phares [4], Alber and Lees [13], and Strahle and Mehta [14] present extensive refinements to the basic Crocco-Lees approach. Although

each differs in significant detail, such as the determination of the turbulence-transport model and the treatment of the inviscid stream, they all exhibit to varying degrees the difficulties of the basic theory as pointed out in Section II. They all, for the most part, give good results for simple flows. The extension to two converging mixing layers is not straightforward.

CHAPTER II

THEORY

I. Basic Considerations

When a turbulent stream separates at the bluff trailing edge of a body, the free tangential shearing surface, being unstable, breaks into eddys which transport matter across the surface creating a mixing zone. The mixing zone is an identifiable region across which the properties of the stream and base gases are distributed. Time-averaged measurements show these distributions as coherent profiles of velocity, temperature, and species concentration. (See Hussain and Zedan [15] and Rhudy and Magnan [16].) After turning toward the lower pressure of the base, the stream must recompress and return to its original direction. Part of the mixing layer will have insufficient energy to overcome the adverse pressure change, and it will remain in the recirculating fluid of the base. If a pure gas, say hydrogen, were bled into the base, the base gas would be a mixture of hydrogen and the free-stream air. In steady flow, the base gas can be considered as a separate, quiescent, homogeneous mixture. The mixing layer would be a distribution, then, from pure base mixture to pure free-stream air at the high-speed edge. At an intermediate point within the layer, the local mixture would be,

say, 40 percent base mixture and 60 percent free-stream air. The base mixture, of course, would contain some free-stream air.

Reynolds-averaged flow is assumed throughout the following analytical development.

II. Key Streamlines

Two streamlines which are important to the evaluation of the global conservation equations are the stagnating streamline, y_S, and the dividing streamline, y_D.

The stagnating streamline is that streamline which separates that part of the flow which continues through recompression (the high-speed part) from that which turns back into the base region (the low-speed part). It is determined by the recompression theory of this chapter in Section VIII.

The dividing streamline is defined simply for mass accounting purposes. It is defined by the following relation:

$$\left[\int_0^{y_U} \rho_s u_s \, dy\right]_{x=o} = \left[\int_{y_D}^{y_U} \rho u \, dy\right]_{x=\ell} . \tag{1}$$

That is, the dividing streamline is that streamline outside of which the mass of the separating flow at the corner is completely accounted for.

III. Open Wake

The open wake was hypothesized by Korst, et al. [1]. It serves to account for the fact that a net mass of fluid is being pumped into and out of the base region by the high-speed streams. With reference to Fig. 2, if the dividing streamline were found on the low-speed side of the stagnating streamline, then part of the mass of the stream before separation is counted as going into the base. The converse situation would have part of the base flow eventually being ushered downstream through recompression. In the limiting case of symmetrical, two-dimensional flow without base bleed, the dividing streamline and the stagnating streamline coincide.

IV. Global Conservation

The global mass balance may now be formulated. In other words, the mass rate of the base flow entrained into the mixing layer must equal the mass rate of that which is turned back into the base region, plus any bleed.

Consider the control volume, A-B-C-D, of Fig. 2 which encloses the base region. The mass flowing inside the dividing streamlines accounts for all the mass of the base region. The mass crossing A-B and C-D is the entrained base mass; so that

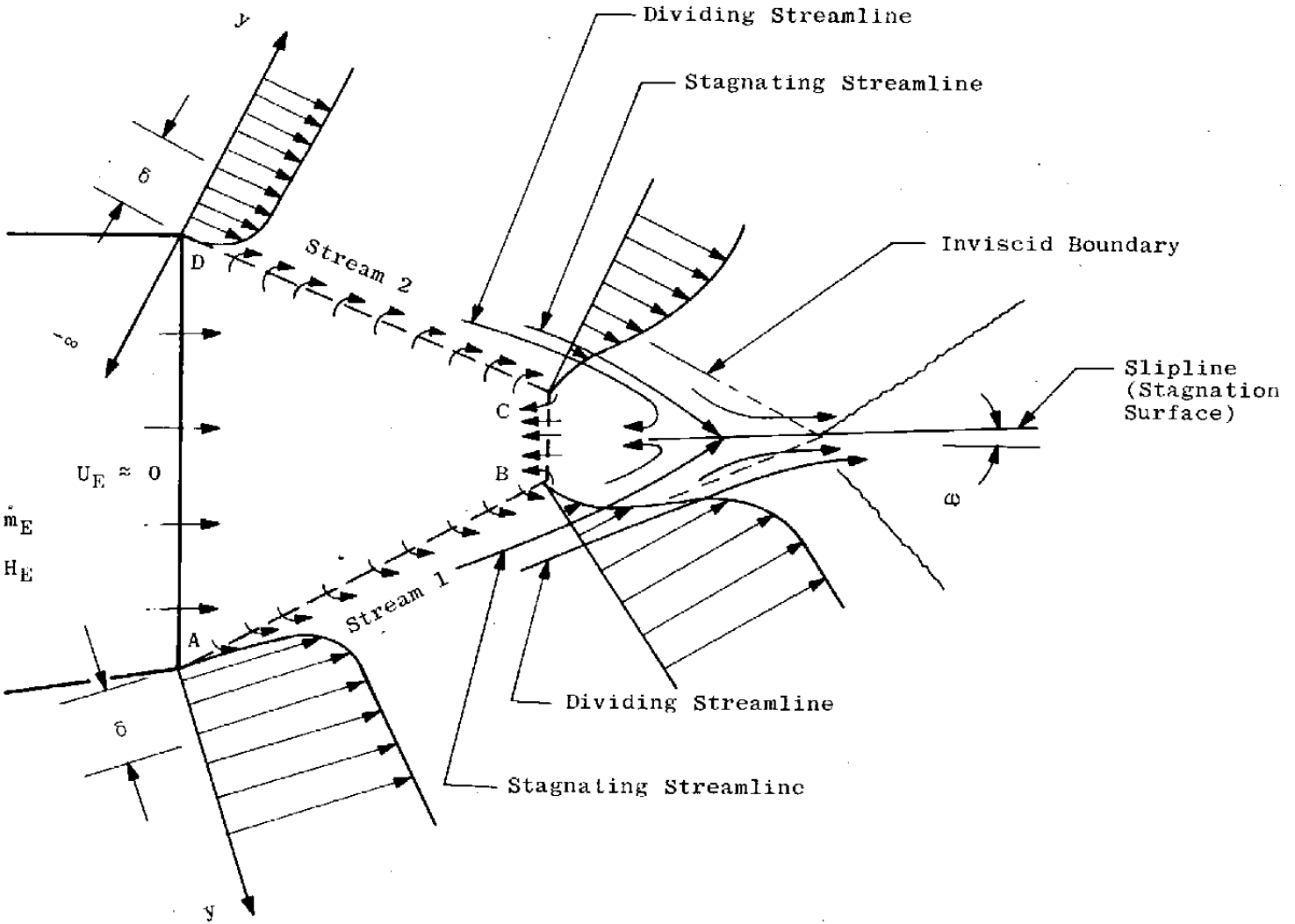

Figure 2. Schematic of flow behavior in near-wake region.

$$\dot{m}_{A-B} + \dot{m}_{C-D} = \left[\int_{y_L}^{y_D} \rho u dy\right]_{S1} + \left[\int_{y_L}^{y_D} \rho u dy\right]_{S2} = \dot{m}_B \quad . \tag{2}$$

The mass entering B-C is accounted for as the total mass flow turned back inside the stagnating streamlines, or

$$\dot{m}_{C-D} = \left[\int_{y_L}^{y_S} \rho u dy\right]_{S1} + \left[\int_{y_L}^{y_S} \rho u dy\right]_{S2} \quad . \tag{3}$$

With bleed flow, the mass conservation equation becomes

$$\left[\int_{y_L}^{y_D} \rho u dy\right]_{S1} + \left[\int_{y_L}^{y_D} \rho u dy\right]_{S2} = \dot{m}_E + \left[\int_{y_L}^{y_S} \rho u dy\right]_{S1} + \left[\int_{y_L}^{y_S} \rho u dy\right]_{S2} \quad . \tag{4}$$

Similarly, the energy equation is

$$H_B\left\{\left[\int_{y_L}^{y_D} \rho u dy\right]_{S1} + \left[\int_{y_L}^{y_D} \rho u dy\right]_{S2}\right\} = \dot{m}_E H_E + \left[\int_{y_L}^{y_S} \rho u H dy\right]_{S1} + \left[\int_{y_L}^{y_S} \rho u H dy\right]_{S2} \quad , \tag{5}$$

where the mass through the base region is assumed, as mentioned, to be a homogeneous mixture of low-velocity gas. As the base-region gas and the bleed are assumed to have negligible velocities, there are sufficient conservation relations for finding two thermodynamic properties of the base such as pressure and enthalpy. However, at this point, the limits of integration are unknown, as are the relationships between the integrands and the variables of

integration. The appropriate relations will be developed in the following.

V. Mixing Analysis

Here the mixing analysis of Korst is followed as detailed by Chapman and Korst [17]. In particular, the general case with initial boundary layer is considered.

Consider the equation of motion of a two-dimensional, constant pressure boundary-layer flow.

$$\rho u \frac{\partial u}{\partial x} + \rho v \frac{\partial u}{\partial y} = \frac{\partial}{\partial y} \left(\varepsilon_o \frac{\partial u}{\partial y} \right) . \tag{6}$$

In turbulent flow, u and v are the time-averaged velocity components, and ε is interpreted as an apparent kinematic viscosity. The equation of motion is reduced using order of magnitude arguments and the assumptions that the apparent viscosity is independent of y and the flow incompressible; that is,

$$\frac{\partial u}{\partial x} = \frac{\varepsilon}{U} \frac{\partial^2 u}{\partial y^2} . \tag{7}$$

By assuming

$$\varepsilon = \varepsilon_o F(x) , \tag{8}$$

Eq. (7) may be cast in the form

$$\frac{\partial u}{\partial \zeta} = \frac{\partial^2 u}{\partial y^2} . \tag{9}$$

The solution to the heat conduction equation is well known (see [18]). It is:

$$u(y,\zeta) = \frac{1}{2\sqrt{\pi\zeta}} \int_{-\infty}^{\infty} e^{-\frac{(y-\beta)^2}{4\zeta}} f_o(\beta)\,d\beta \ , \qquad (10)$$

where $f_o(\beta)$ is the initial condition. From Fig. 2, it is apparent that the initial profile is zero from minus infinity to zero. From zero to the boundary-layer thickness, δ, it is the boundary-layer profile. From δ to $+\infty$, the profile is that of the expanded free stream. Applying this initial profile,

$$u(y,\zeta) = \frac{U}{2}\left\{1 + \operatorname{erf}\left[\frac{(y-\delta)}{2\sqrt{\zeta}}\right]\right\} + \frac{1}{2\sqrt{\pi\zeta}} \int_{o}^{\delta} e^{-\frac{(y-\beta)^2}{4\zeta}} u_s(\beta)\,d\beta \qquad (11)$$

is obtained.

It is well known that when the mixing region is fully developed, that is, when δ/x is very small, that the velocity profile is well approximated by

$$u = \frac{U}{2}\left[1 + \operatorname{erf}\left(\frac{\sigma y}{x}\right)\right] \ , \qquad (12)$$

where σ is a constant usually referred to as the spreading parameter, which is experimentally determined. Using this fact, the velocity profile may be written as

$$u(\eta) = \frac{U}{2}\left[1+\operatorname{erf}(\eta-\eta_p)\right] + \frac{\eta_p}{\sqrt{\pi}}\int_0^{1.0} e^{-\left[\eta-\eta_p\left(\frac{y}{\delta}\right)\right]^2} u_s\left(\frac{y}{\delta}\right) d\left(\frac{y}{\delta}\right), \quad (13)$$

where

$$\eta = \frac{\sigma y}{x}$$

and

$$\eta_p = \frac{\sigma\delta}{x} \quad . \quad (14)$$

This implies that the kinematic viscosity, ε, is a linear function of x.

VI. Determination of y_m

The limits of integration y_U and y_L as used in Eq. (1) are functions of distance from the inception of mixing. The upper limit is taken as that point where the velocity ratio, u/U, is 0.99998895. The lower limit is taken where u/U is 0.00001105. Thus, the actual y value changes as the mixing zone spreads into the inviscid flow. At a particular distance from the inception of mixing, if the particular inviscid streamline at y_U were traced back to the beginning, the momentum of the mixing zone should account for the momentum of the initial profile out to that streamline. Because of simplifications of the theory, however, the momentums will not check. So as to balance the momentum, the upper limits on the integrals are extended by y_m, which is not a coordinate, but an increment; so that

$$\int_0^{y_U} \rho_s u_s^2 dy \Big]_{x=o} = \int_{y_L}^{y_U+y_m} \rho u^2 dy \Big]_{x=\ell} . \qquad (15)$$

Korst and his co-workers also consider the profile to have shifted by a like amount so that the inviscid boundary no longer is located at the half-velocity point of the fully developed profile, but at $y = y_m$. As this shift causes the profiles to align better with experimental profiles, this localization with respect to the inviscid boundary is adopted here. The transverse coordinate is always fixed at the half-velocity point of the fully developed profile wherever the profile may fall. Thus, y_m is completely determined by Eq. (15).

VII. Constitutive Equations

Mass Fractions of the Streams in the Base

To be able to determine the base mixture, the mass fractions of the primary streams and the bleed gas in the base must be determined. As the base mixture is determined by the fact that distributed mixtures (the mixing layers) are being turned back into the base, the functional form of the species distribution must be determined before proceeding.

If the assumption of no initial boundary layer is made, as in [19], then by assuming unity turbulent Prandtl and Lewis numbers, the species and total-enthalpy-distribution profiles can be taken as the same as the velocity

profile. However, in the situation being investigated here, the initial species profile is a step function; whereas the velocity profile is that of the boundary layer. By assuming a species distribution function as

$$k = \frac{1}{2}\left[1 + \mathrm{erf}(C_{mf}\eta)\right], \tag{16}$$

with the shape parameter, C_{mf}, to be determined, the disparity between the profiles is accommodated. The species profile, which has larger gradients, is always approaching the velocity profile as the mixing develops. (This is borne out in the computations which calculate C_{mf} to be always greater than unity except in the fully developed limit where it is, of course, unity.)

The C_{mf} parameter is determined by a mass balance, as

$$\left[\int_o^{y_U} \rho_s u_s dy\right]_{x=o} = \left[\int_{y_L}^{y_U+y_m} k\rho u dy\right]_{x=\ell} . \tag{17}$$

Thus, with Eq. (15) as

$$\left[\int_o^{y_U} \rho_s u_s^2 dy\right]_{x=o} = \left[\int_{y_L}^{y_U+y_m} \rho u^2 dy\right]_{x=\ell} , \tag{18}$$

there are two equations for the two unknowns, C_{mf} and y_m.

Then the mass fraction of Stream 1 gas in the base mixture is

$$mf_1 = \frac{\int_{y_L}^{y_S} k\rho u dy\,]_{S1} + mf_1 \left\{ \int_{y_L}^{y_S} (1-k)\,\rho u dy\,]_{S1} + \int_{y_L}^{y_S} (1-k)\,\rho u dy\,]_{S2} \right\}}{\dot{m}_E + \int_{y_L}^{y_S} \rho u dy\,]_{S1} + \int_{y_L}^{y_S} \rho u dy\,]_{S2}} , \qquad (19)$$

or

$$mf_1 = \frac{\int_{y_L}^{y_S} k\rho u dy\,]_{S1}}{\dot{m}_E + \int_{y_L}^{y_S} k\rho u dy\,]_{S1} + \int_{y_L}^{y_S} k\rho u dy\,]_{S2}} . \qquad (20)$$

Also for Stream 2,

$$mf_2 = \frac{\int_{y_L}^{y_S} k\rho u dy\,]_{S2}}{\dot{m}_E + \int_{y_L}^{y_S} k\rho u dy\,]_{S1} + \int_{y_L}^{y_S} k\rho u dy\,]_{S2}} , \qquad (21)$$

and for the bleed gas,

$$mf_E = 1 - mf_1 - mf_2 .$$

Thus, having the mass fractions of the respective stream in the base, sufficient information is available to determine the base-gas mixture and its properties.

Chemical Equilibrium Considerations

In any compressible flow analysis, a thermal equation of state is required to close the system of equations, such as

$$\rho = \rho(p,h) \quad . \tag{22}$$

A caloric equation of state is also required since empirically determined properties are expressed as functions of temperature, so that

$$t = t(p,h) \quad . \tag{23}$$

The requirement of the equilibrium chemistry analysis, then, is that it supply the required functional relations.

The mixture is assumed to be composed of thermally perfect gases; so that the thermal equation of state is

$$\rho = \frac{p}{t}\left[\frac{\sum_i C_i w_i}{\hat{R}}\right] \quad . \tag{24}$$

The caloric equation is of the form

$$h = \frac{\sum_i \left[\int_o^t C_i c_{p_i}\, dt + C_i h_i^{\,o}\right]}{\sum_i C_i w_i} \quad , \tag{25}$$

which assumes that each species behaves ideally. The zero superscript denotes a known evaluation of the variable at reference (zero temperature) conditions. To evaluate these

relations requires c_{p_i} for each species present as a function of temperature and the mole fraction of each species present.

Reference [20] provides a functional form for the various properties of 210 substances to 6000°K. For example, the specific heat at constant pressure is given as

$$\frac{c_{p_i}}{\hat{R}} = a_1 + a_2 t + a_3 t^2 + a_4 t^3 + a_5 t^4 \quad . \tag{26}$$

But to make the problem simpler, this reference also provides, directly, $h_i = h_i(t)$ as well as entropy and the Gibbs function per mole. All that is further required, then, are the mole fractions, C, of the species present.

In general, in a given mixture of m atoms and n species, the following relations hold. For example, see [21]. For a given mixture there are n-m equilibria

$$\sum_j \alpha_{ij} X_j \rightleftarrows \beta_{ij} X_j \qquad i = 1, n-m \quad , \tag{27}$$

with the corresponding mass-action relations as

$$K_i = \prod_j (p_{ij})^{(\beta_{ij}-\alpha_{ij})} = \exp\left[\frac{-\sum_j (\beta_{ij}-\alpha_{ij})\mu_{ij}^{o}}{\hat{R}t}\right] \begin{matrix} i=1, n-m \\ j=1, n \end{matrix} \quad , \tag{28}$$

and m atom conservation equations

$$\sum_{j} a_{kj} p_{kj} = P_k \qquad \begin{matrix} k=1, m \\ j=1, n \end{matrix} , \tag{29}$$

where P_k is the fictitious partial pressure of the kth atom.

The Gibbs free energy per mole of individual species is given by [20] in functional form as mentioned. These n equations are sufficient to solve for the n partial pressures of species present and, along with the known pressure of the mixture, to determine the mole fractions of the species. It is possible, then, for a given mixture of atoms to determine any state variable required as a function of pressure and enthalpy. Appendix A shows by example the method of determining the mole fractions.

Flame Sheet

At this point, it is necessary to examine the flame-sheet concept as implemented by Davis [19]. This concept is attributed to Abramovich [22], and Libby [23]. The primary assumption of the model is that combustion occurs along an infinitely thin layer within the mixing region. At this point, the concentrations of fuel and oxidizer are taken to be zero, but the amounts consumed in the reaction are in stoichiometric proportion. The concentration of fuel on the lean side of the flame is zero as is the oxidizer on the rich side. In Davis' case, he

considers only the hydrogen/oxygen reaction of his experiment. By assuming a Crocco relation between the velocity profile and the atomic species distribution, he is able to determine the stoichiometric point in the mixing layer, then distribute the products of combustion on either side of the flame front using the Crocco relation and the concentration assumption on the fuel and oxidizer as stated above. Although no motivation is given by Davis for this approach, it is quite apparent that the need to solve the mass-action equations and atom-conservation equations for the equilibrium concentrations of each species has been obviated. The principal objection, though, to Davis' approach is that he disallows oxygen to be present in the base mixture. This would bring into question Davis' analysis of the cases with little hydrogen bleed, which have base mixtures on the lean side of the stoichiometric point.

In conclusion, it can be said that Davis' chemistry model is a relatively good approximation for mixing layers between streams of pure fuel and oxidizer. In the base-flow problem, these conditions do not obtain because of the recirculation into the base of significant portions of the oxidizer stream.

VIII. Recompression Analysis

General Considerations

Korst's original analysis did not contain a recompression model as such; rather, he simply assumed that the

stagnating or discriminating stream isentropically stagnated at the static pressure downstream of the recompression shock. Experiments showed this to be incorrect. To account for this fact, others such as Nash [10], and Addy [11] devised empirically determined recompression factors. These were unsatisfactory as they could only correlate existing data rather than predict.

Bauer and Fox [2], however, devised an analytical model which obviated the requirement for a recompression factor. Their approach, however, overpredicted the base pressure for thick boundary layers. This was because they used essentially an inviscid analysis to determine the extent of the recompression region.

In the present work, a novel approach is used for modeling the recompression process.

Approach

Determination of the location of the stagnating streamline, y_S, is tied to the recompression process where the two streams merge, turn, and recompress to the ambient pressure. Figure 3 isolates one of the impinging streams.

The base flow is assumed to turn back through an area equal to the approaching area between y_S and y_L; thus, the beginning of recompression, X_1, is related to y_S geometrically. Reference [2] showed the function,

$$\frac{p - p_B}{p_r - p_B} = \sin^2 \left[\frac{\pi}{2} \left(\frac{X - X_1}{X_2 - X_1} \right) \right] , \qquad (30)$$

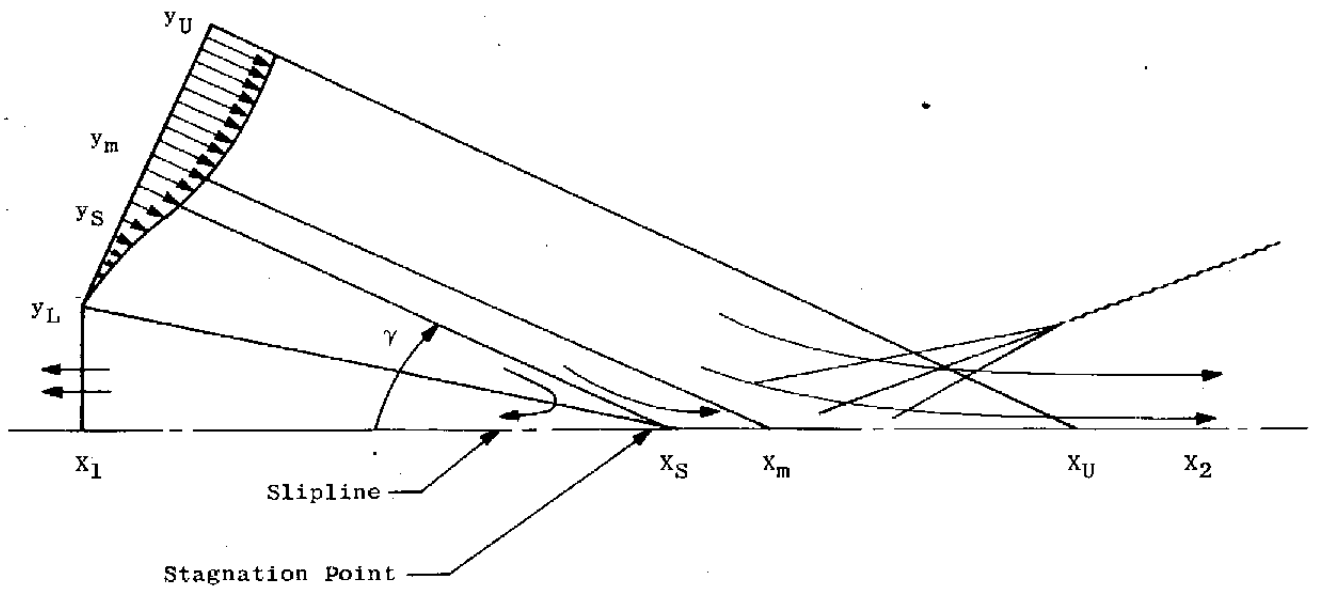

Figure 3. Schematic of recompression region.

to be a good fit of recompression data. The downstream pressure, p_r, is that resulting from the inviscid calculation of shock and slipline. The actual recompression process on the slipline is stretched out as indicated by Eq. (30). The end of the recompression process, X_2, is approximately determined from simple momentum considerations.

It is assumed that the force due to the pressure rise on the slipline is equal to the transverse momentum given up by the oncoming viscous layer, with all other effects being of negligible importance. This leads to the relation

$$\int_{X_1}^{X_2} p\,dX = \sin\gamma \left[\int_{y_L}^{y_U+y_m} \rho u^2 dy \right]_{x=\ell} + p_B \left(X_U - X_1 \right) , \qquad (31)$$

where

$$X_U = X_m + \left(y_U - y_m \right) / \sin\gamma . \qquad (32)$$

For the backward-facing step problem, Peters and Phares [4] show that the total pressure on the dividing streamline changes little up to stagnation, thus the stagnation process can be approximated as isentropic. The stagnating streamline is determined by finding that stagnation pressure in the oncoming mixing layer which is equal to the static pressure of the recompression region at

the stagnation point, X_S. The recompression pressure at stagnation, p_S, is

$$\frac{p_S - p_B}{p_r - p_B} = \sin^2 \left[\frac{\pi}{2} \left(\frac{X_S - X_1}{X_2 - X_1} \right) \right] \quad ; \tag{33}$$

also

$$h_S = H_S - u_S^2/2 \ ,$$

$$s = s\,(p_B,\ h_S) \ , \tag{34}$$

and

$$s = s\,(p_S,\ H_S) \ ,$$

where u_S and H_S are functions of y_S through the assumed profiles, and y_S and X_S are related by the geometry (Fig. 3). The above relations, then, are sufficient for determining the stagnating streamline as a function of base pressure.

IX. Spreading Parameter for Turbulent Mixing

General

Perhaps one of the most important aspects of any mixing analysis is the determination of the spreading or mixing parameter, σ. As Davis [19] points out, the experimental data are exiguous for jet mixing with combustion. For isoenergetic mixing, the most widely used relation is that due to Korst and Tripp [24],

$$\sigma = \sigma_o + 2.758\ M_U \ , \tag{35}$$

where σ_o is the incompressible spreading parameter. Channapragada [25] presented a relation using a mixing length argument which attempts to account for density variation as

$$\sigma = \sigma_o \left[B \left(\frac{\rho_U + \rho_B}{\rho_U} \right) \right]^{-1} \ , \tag{36}$$

where B is a correlation factor that has values of from 0.5 to 0.25 as Mach number increases from zero to above 3.0. Abramovich presented a relation that reduces to

$$\sigma = 2\sigma_o \left(1 + \rho_B / \rho_U \right)^{-1} \tag{37}$$

for mixing with a quiescent base gas.

Prandtl's Mixing Length Model

The most satisfactory model for this analysis, however, is that of Bauer [26] who ties the Prandtl mixing-length hypothesis directly to the integral approach of the Korst theory.

Considering the fully developed profile of Fig. 4 and using a control volume approach, it is apparent that

$$\int_0^{\ell} \tau_D d\ell = \int_{y_L}^{y_D} \rho u^2 dy \tag{38}$$

from a momentum balance. Any viable shear stress model

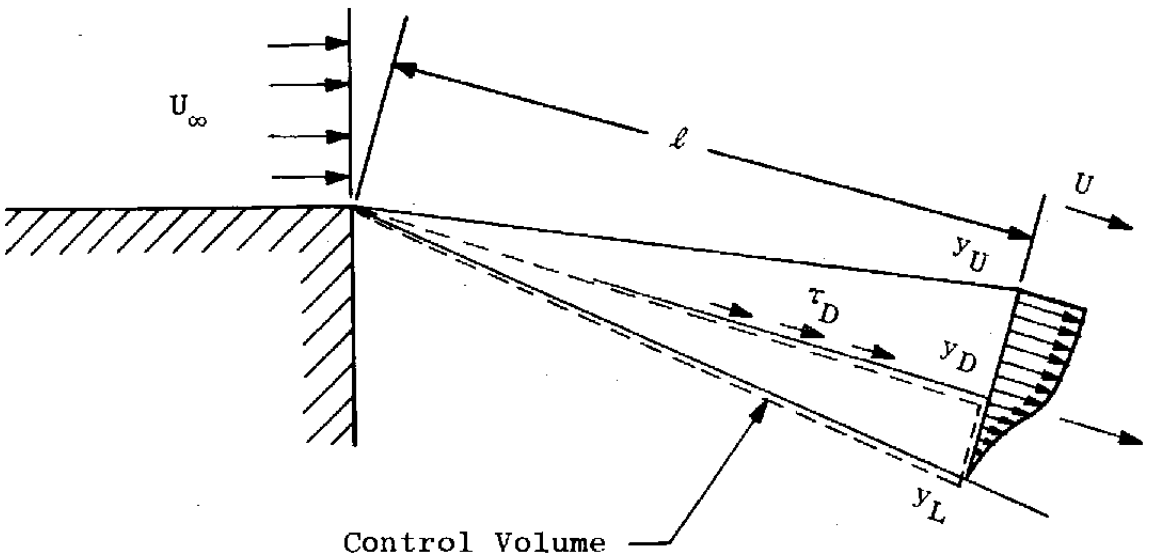

Figure 4. Isolation of control volume in typical mixing zone.

could be used for τ_D. However, in this approach, the Prandtl mixing-length model is used as

$$\tau_D = \rho_D \bar{\ell}^2 \left(du/dy \right)_D^2 . \tag{39}$$

It is assumed that the mixing length is proportional to the local mixing zone width:

$$\bar{\ell} = 2\eta_U \bar{k} \ell / c \tag{40}$$

or

$$\tau_D = 4\eta_U^2 \bar{k}^2 \rho_D \left(du/d\eta \right)_D^2 . \tag{41}$$

Substituting into Eq. (38) and performing the integration,

$$\sigma = \int_{\eta_L}^{\eta_U} \frac{\rho}{\rho_U} \phi^2 d\eta \; / \; \left[C_k \left(\frac{d\phi}{d\eta} \right)_D^2 \right] \tag{42}$$

is obtained. The constant, C_k is determined by [26] as $0.5085/\sigma_o$.

A comparison of the various theories is presented in Fig. 5 with σ_o as 12.0. As is pointed out by Birch and Eggers [27], the data follow two distinct curves. The main difference in the data is Reynolds number: the lower data curve having, in general, the lower Reynolds number. The best model for the present analysis is, as mentioned, the lowest curve [26]. It changes the least with Mach number. It seems that base flows in particular require the flat

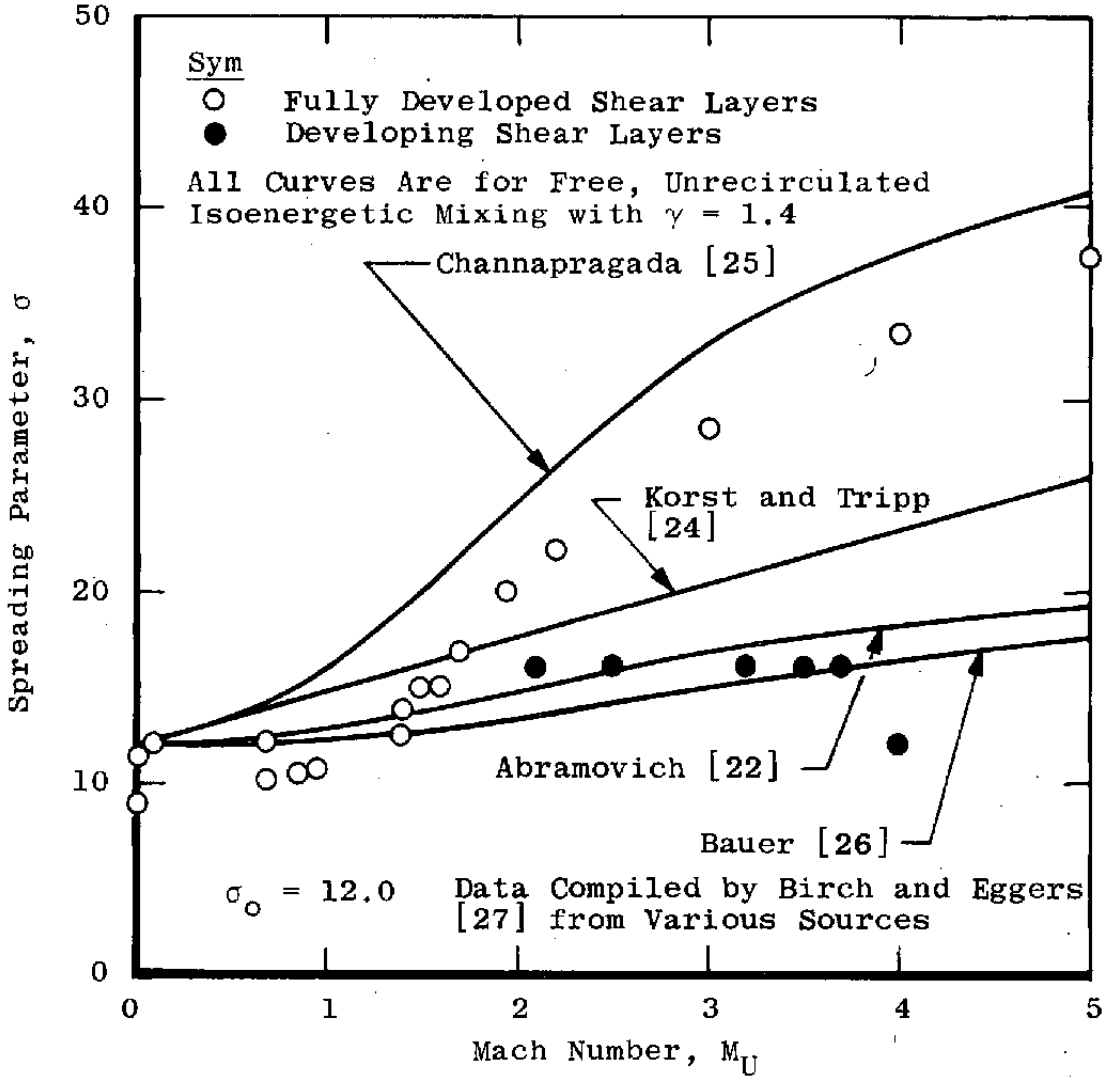

Figure 5. Comparison of the various spreading parameter models.

trajectory. It is as though the entrained flow from the base retained a memory of its turbulent past, which serves to increase mixing against the opposite trend of the Mach number effect for the mixing of flows which have not been recirculated.

It must also be pointed out that the reference value of 12.0 is for developed flows. Most base flows are not fully developed. Hussain and Zedan [15] indicate that the history of the initial boundary layer has a significant effect on the developing σ_o. Their experiments show that, for a boundary layer that has been tripped, the mixing parameter takes between one and two nozzle radii to reach a value of nine. Consequently, σ_o was taken as nine in all flows except those involving bleed with burning where a value of twelve was used because of convergence problems with the value of nine.

Using a σ_o of nine with the mixing-length theory gives values of the computed mixing parameter that range in value from 9.0 to about 13.5 for the isoenergetic problems. This is consistent with the constant value of 12.0 which is used by others such as Strahle and Mehta [14], and Chow and Spring [8]. In fact, a constant value of 12.0 would work quite well for the present work.

X. Correction for Axially Symmetric Effects

The theory as developed is for two-dimensional flows. Extending the Korst analysis with initial boundary

layer to axially symmetric flow is not obvious. In particular, the procedure for determining the profile shift is not developed in the literature. A suggested approach is developed in Appendix B; but, at this point, it appears costly in computational time.

However, as the two-dimensional theory is an approximation and gives good results, it is reasonable to attempt to approximate the axially symmetric effects. The first approach attempted was that used in [2].

Bauer [28] showed that for a zero initial boundary layer, under circumstances that prevail in many of the flows of interest, the two-dimensional mixing analysis is a good approximation for axially symmetric flows if

$$\frac{\sigma R_i}{\ell \cos \beta} > 10 \quad . \tag{43}$$

This condition holds for the flows under consideration in this study. It is reasonable to assume that the inclusion of the initial boundary layer would not alter this condition.

Reference [2] also used a new spreading rate parameter which was adjusted to account for the difference in spreading between axially symmetric mixing and two-dimensional mixing. This is derived in [2] as

$$\sigma_A = \overline{\sigma} \left(\frac{2R_i}{R_s + R_i} \right) , \tag{44}$$

where the bar serves to distinguish the two-dimensional variables for this discussion. Reference [2] goes further and assumes that the variation in radius across the mixing layer is small and can be removed from beneath the integral sign. This has the effect of making the global conservation equations identical to those in two-dimensional flow when no bleed is present. The theory is summarized in the following.

1. The inviscid field is determined from the axially symmetric method of characteristics.
2. The mixing theory and the recompression process are treated as two-dimensional except as modified by a new σ.
3. The global conservation equations are two-dimensional except as modified by the new σ.

While the assumption of essentially two-dimensional mixing may be justified by the nature of the mixing and the fact that it is removed from the centerline, it is not as clear that the mixing layer may be considered thin as regards the recompression process and the global conservation.

Consequently, a second approximation was implemented whereupon the global conservation relations and the recompression relations were replaced by their axially symmetric counterparts. Typically, for mass conservation,

$$2\pi \left[\int_{y_L}^{y_D} \rho u R dy \right]_{S1} + 2\pi \left[\int_{y_L}^{y_D} \rho u R dy \right]_{S2} = \dot{m}_E + 2\pi \left[\int_{y_L}^{y_S} \rho u R dy \right]_{S1} + 2\pi \left[\int_{y_L}^{y_S} \rho u R dy \right]_{S2} , \quad (45)$$

and for the recompression momentum balance,

$$2\pi \int_{X_1}^{X_2} p R dX = 2\pi \sin\gamma \int_{y_L}^{y_U+y_m} \rho u^2 R dy + \pi p_B (R_U + R_1)(X_U - X_1) . \quad (46)$$

A third approximation is considered which is based on the familiar Mangler transformation. Consider first that the entire two-dimensional approximation is based on a solution of the simplified boundary-layer equations. For laminar flow, the well-known Mangler transformation (see Tetervin [29]) transforms the axisymmetric boundary-layer equations into the two-dimensional boundary-layer equations exactly. For a free boundary, the transformation is

$$\begin{aligned} \bar{x} &= \int^{x} \left(\frac{R_i}{L} \right)^q dx , \\ \bar{y} &= \frac{R_i}{L} y , \\ \bar{\rho}\,\bar{u}(\bar{x}) &= \rho u(x) , \\ \bar{\rho}_U \bar{U}(x) &= \rho_U U(x) , \end{aligned} \quad (47)$$

and

$$\rho v = \frac{R_i}{L} (\bar{\rho}\,\bar{v}) - \bar{\rho}\,\bar{u}\,\frac{L\bar{y}}{R_i^2}\,\frac{dR_i}{dx} ,$$

where R_i is the radius of the inviscid boundary and L is a reference length. As the two-dimensional analysis gives good results, the question is: would this simple transformation give a good axisymmetric approximation?

Reference [29] points out that the standard transformation with a q of two is not exact for turbulent flow; but, for low turbulence levels and boundaries with slight curvature, it is a good approximation.

The difficulty arises when transforming the term $\partial\tau/\partial y$. Tetervin shows that if the exponent in the integrand of the transformation on x is two, then

$$\frac{\tau}{\bar{\tau}} = \frac{R_i}{L} \quad . \tag{48}$$

This corresponds to laminar flow or flows with low turbulence levels. As the turbulence increases without limit,

$$\frac{\tau}{\bar{\tau}} \to 1 \quad , \tag{49}$$

which corresponds to an exponent of unity on the integrand of the x transformation. In this instance, it is a simple matter to determine the relationship between the spreading parameters also.

Consider the control volume of Fig. 4, page 34.

Let

$$\tilde{R} = \frac{\int_{y_L}^{y} \rho u^2 R dy}{\int_{y_L}^{y} \rho u^2 dy} \quad ; \tag{50}$$

then,

$$2\pi \int_{o}^{x} \tau_o R dx = 2\pi \tilde{R}_o \int_{y_L}^{y_o} \rho u^2 dy \quad . \tag{51}$$

Now, as τ_o is independent of R for high turbulence levels,

$$\tau_o \left(\frac{R_s + R_o}{2} \right) = \tilde{R}_o \rho_U U^2 \frac{1}{\sigma_A} \int_{\eta_L}^{\eta_o} \frac{\rho}{\rho_U} \phi^2 d\eta \quad . \tag{52}$$

For a two-dimensional mixing layer

$$\bar{\tau}_o = \rho_U U^2 \frac{1}{\bar{\sigma}} \int_{\eta_L}^{\eta_o} \frac{\rho}{\rho_U} \phi^2 d\eta \tag{53}$$

or

$$\frac{\tau_o}{\bar{\tau}_o} = \frac{2\tilde{R}_o}{R_s + R_o} \frac{\bar{\sigma}}{\sigma_A} \approx 1 \quad . \tag{54}$$

Then

$$\sigma_A = \frac{2\tilde{R}_o}{R_s + R_o} \bar{\sigma} \quad . \tag{55}$$

If R_o is taken at the inviscid boundary and R_i is considered a good approximation to $\tilde{R}$, then

$$\sigma_A = \left(\frac{2R_i}{R_s + R_i}\right)\bar{\sigma} \quad , \tag{56}$$

which is exactly Eq. (44). The Mangler transformation for this case gives

$$\eta = \frac{\bar{\sigma}\bar{y}}{\bar{x}} = \bar{\sigma}\left(\frac{R_i}{L}\right)\frac{Ly}{\int_o^x R_i dx} \tag{57}$$

or

$$\eta = \bar{\sigma}\left(\frac{2R_i}{R_s + R_i}\right)\left(\frac{y}{x}\right) \tag{58}$$

for a conical boundary.

Thus, the modification to $\bar{\sigma}$ given by Eq. (44) can be interpreted as the Mangler transformation for highly turbulent flow.

For slightly turbulent flow and an exponent of two,

$$\eta = \bar{\sigma}\,\frac{3R_iR_s}{R_i^2 + R_iR_s + R_s^2}\left(\frac{y}{x}\right) \quad , \tag{59}$$

where a reference length of R_s was used to be consistent with Eq. (57). That is, for the case of an inviscid boundary parallel to the axis of symmetry where $R_i = R_s$, there is no distortion of the spreading parameter.

Dixon, et al. [30] also consider R_s to be appropriate as the reference length.

XI. Inviscid Field

Basic Method of Characteristics

The general inviscid flow field is developed using the classical method of characteristics. A presentation of the details of the method is given by Fox [31]. An interesting derivation of the method is given in Appendix C. Starting with the axially symmetric, inviscid conservation equations of mass, axial and radial momentum, and energy, as

$$\rho v + r \frac{\partial \rho v}{\partial r} + r \frac{\partial \rho u}{\partial z} = 0 ,$$

$$\rho u \frac{\partial u}{\partial z} + \rho v \frac{\partial u}{\partial r} + \frac{\partial p}{\partial z} = 0 , \qquad (60)$$

$$\rho u \frac{\partial v}{\partial z} + \rho v \frac{\partial v}{\partial r} + \frac{\partial p}{\partial r} = 0 ,$$

and

$$\rho u \frac{\partial H}{\partial z} + \rho v \frac{\partial H}{\partial r} = 0 .$$

With the definition of total enthalpy as

$$H = \frac{1}{2} (u^2 + v^2) + h , \qquad (61)$$

the well-known ordinary differential equations of the method are derived as

$$udr - vdz = 0 \qquad (62)$$

and

$$(u^2 - a^2)\,dr^2 - 2uvdrdz + (v^2 - a^2)\,dz^2 = 0 \qquad (63)$$

for the characteristic surfaces. The compatibility relations along the first surface which is a streamline are

$$dp/\rho + udu + vdv = 0 \qquad (64)$$

and

$$dh + udu + vdv = 0 \ . \qquad (65)$$

The compatibility relations along the second set of surfaces, which are the left and right-running characteristics, are

$$(udr - vdz)(udz - vdu) + (udr - vdz)^2\, v/r + dp/\rho\,(vdr + udz) = 0 \qquad (66)$$

The equations are put in finite-difference form and integrated numerically subject to the conditions at the plume boundary. As the plume boundary is a free surface, the conditions are:

1. The surface is a streamline.
2. The pressure is constant along the surface.

Also, there are particular features of the flow field that require special treatment, as detailed below.

Embedded Shock

The embedded shock within the plume is treated in detail in [31]; consequently, only an overview will be presented here.

The shock wave occurs in the solution field when characteristic curves of the same sense coalesce and overlap one another. Double-valued points occur. A shock discontinuity is inserted to match the low-pressure core region to the high-pressure boundary region. The conservation equations across the shock reduce to

$$\begin{aligned} \rho_2 u_2 \sin\beta + \rho_2 v_2 \cos\beta &= \rho_1 u_1 \sin\beta + \rho_1 v_1 \cos\beta = C_1 \ , \\ C_1 u_2 + p_2 \sin\beta &= C_1 u_1 + p_1 \sin\beta \ , \\ C_1 v_2 + p_2 \cos\beta &= C_1 v_1 + p_1 \sin\beta \ , \end{aligned} \tag{67}$$

and

$$h_2 + \frac{u_2^2}{2} + \frac{v_2^2}{2} = h_1 + \frac{u_1^2}{2} + \frac{v_1^2}{2} \ ,$$

where the subscript "1" refers to known upstream conditions, the "2" refers to the downstream conditions to be found, and β is the angle between the shock and the axial direction, measured clockwise positive.

Corner Expansion

At the corners encountered both by the plume and the outer stream, the flow must turn abruptly to match the base pressure. In an inviscid flow, the flow properties at the point of expansion are not single valued; that is, the field at that point is assumed to experience a continuous change in pressure from the pressure existing before the turn to the pressure of the base region. The required relations, valid at a point, are called the Prandtl-Meyer

relations. They can be shown to be the limiting forms of the compatibility relations along both a characteristic and a streamline as the coordinate differentials, dr and dz, go to zero. They are

$$\frac{du}{dp} = \frac{-\frac{u}{\rho} + v\frac{\sqrt{M^2-1}}{\rho}}{u^2 + v^2} \tag{68}$$

and

$$\frac{dv}{dp} = \frac{-\frac{u}{\rho}\sqrt{M^2-1} - \frac{v}{\rho}}{u^2 + v^2} \quad . \tag{69}$$

Thus, the velocities can be determined as a function of pressure at a point.

Recompression Shocks at the Intersection of the Streams

Figure 6 is a more detailed representation of the recompression region resulting from the intersection of the two streams. The downstream side of both shock waves must match flow angle and pressure along the slipline separating the two flows. Therefore,

$$\left.\frac{v_2}{u_2}\right]_{S1} = \left.\frac{v_2}{u_2}\right]_{S2} \tag{70}$$

and

$$\left.p_2\right]_{S1} = \left.p_2\right]_{S2} \quad . \tag{71}$$

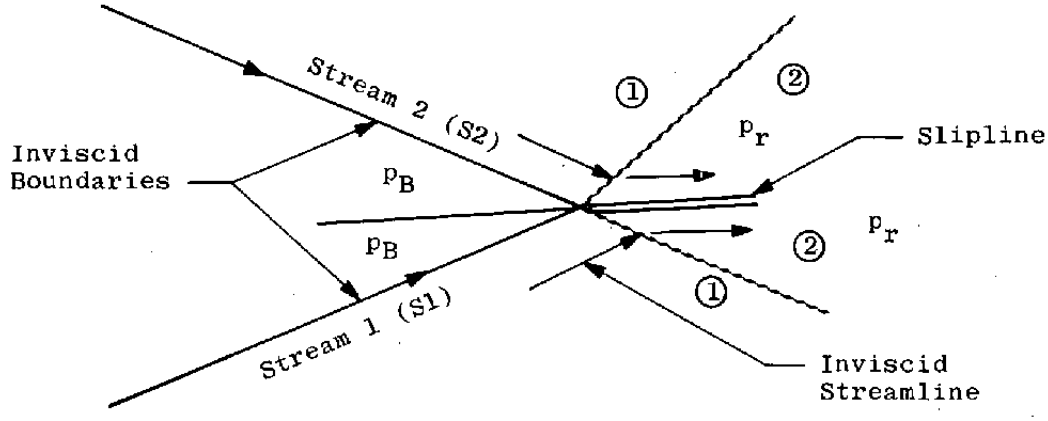

Figure 6. Detail of inviscid recompression.

These two relations coupled with two sets of shock relations, Eq. (67), are sufficient to solve for the flow parameters along the slipline downstream of the shock.

Thus, given the initial conditions upstream of the corners for both streams and the pressure in the base region, the inviscid boundaries are developed in a marching scheme using the method of characteristics until the intersection point with the recompression region is determined.

CHAPTER III

SOLUTION PROCEDURES

I. Introduction

In Chapter II the overall theory for the separation, mixing, and compression of turbulent viscous layers was presented along with that of the corresponding inviscid field. It is the purpose of the following sections to show in an unambiguous way the solution procedure used to determine the base properties when two different supersonic streams (the air stream and the rocket exhaust in the most general case) separate, mix with the base gas, and recompress to the downstream pressure. The principal assumption employed is that the two layers do not interact except as they both impact and turn upon an imaginary slipline. The slipline is determined completely by the inviscid computations using the method of characteristics. The mixing and recompression processes of the two mixing layers are assumed to occur independently of one another, having only the base pressure in common. The two mixing fields are coupled only through the global conservation relations. All of the terms of the global relations, except the bleed terms, are evaluated at the inviscid intersection. The initial boundary layer is assumed to experience no distortion from the corner expansion process.

II. General Approach

The primary system of equations to be solved is: the conservation of mass

$$2\pi \int_{y_L}^{y_D} \rho u R dy \Big]_{S1} + 2\pi \int_{y_L}^{y_D} \rho u R dy \Big]_{S2} = \dot{m}_E + 2\pi \int_{y_L}^{y_S} \rho u R dy \Big]_{S1} + 2\pi \int_{y_L}^{y_S} \rho u R dy \Big]_{S2} \quad (72)$$

and the conservation of energy

$$2\pi \int_{y_L}^{y_S} \rho u H R dy \Big]_{S1} + 2\pi \int_{y_L}^{y_S} \rho u H R dy \Big]_{S2} + \dot{m}_E H_E$$

$$= H_B \left(2\pi \int_{y_L}^{y_D} \rho u R dy \Big]_{S1} + 2\pi \int_{y_L}^{y_D} \rho u R dy \Big]_{S2} \right), \quad (73)$$

with the unknowns being p_B and H_B. It is convenient to use the mass fractions

$$mf_1 = \frac{2\pi \int_{y_L}^{y_S} k \rho u R dy \Big]_{S1}}{\dot{m}_E + 2\pi \int_{y_L}^{y_S} k \rho u R dy \Big]_{S1} + 2\pi \int_{y_L}^{y_S} k \rho u R dy \Big]_{S2}}, \quad (74)$$

$$mf_2 = \frac{2\pi \int_{y_L}^{y_S} k \rho u R dy \Big]_{S2}}{\dot{m}_E + 2\pi \int_{y_L}^{y_S} k \rho u R dy \Big]_{S1} + 2\pi \int_{y_L}^{y_S} k \rho u R dy \Big]_{S2}}. \quad (75)$$

and the Crocco relation between species distribution and the local total enthalpy as

$$H = kH_1 + (1 - k)\, H_B \tag{76}$$

for the mixing layer of Stream 1, and

$$H = kH_2 + (1 - k)\, H_B \tag{77}$$

for that of Stream 2, to reduce the energy equation to

$$H_B = H_1\, mf_1 + H_2\, mf_2 + (1 - mf_1 - mf_2)\, H_E . \tag{78}$$

For ease of computation, Eqs. (72), (74), and (75) are taken as primary with the unknowns being p_B, mf_1, and mf_2. With no bleed flow, they reduce to two equations and two unknowns p_B and mf_1.

They are solved using the classical Newton-Raphson technique with numerical derivatives. (See [32].)

Although the solution of the system is simple, the evaluation of the terms is tedious. It would be unproductive to reproduce here the many calculations involved as they use no novel numerical techniques.

III. Computational Scheme

To begin, the problem must be defined through a set of geometric, thermodynamic, and fluid dynamic parameters.

Geometric

1. Radius and half-angle of the nozzle.
2. Radius of the afterbody.

Thermodynamic

1. Relative mole-atoms of carbon, hydrogen, nitrogen, oxygen, and argon in Stream 1 and Stream 2 and in the bleed gas.
2. Total enthalpies and pressures of the streams.

Fluid Mechanical

1. Exit static pressure of nozzle.
2. Boundary-layer thickness at exit of nozzle.
3. Static pressure of free stream.
4. Boundary-layer thickness at separation on afterbody.

Then to begin computation, the first guess of base pressure and mass fractions of the streams in the base must be provided.

Inviscid Flow

As the total conditions for each stream are known, the entropy for each stream can be calculated. At constant entropy, the streams are expanded to the base pressure where the gas properties of the two streams are determined. The starting lines are then determined for the method of characteristics. The method of characteristics, using the frozen equilibrium gas properties, provides the entire

inviscid flow field. Most importantly, it allows the length of the inviscid boundary to the point of intersection of the rocket stream and the free stream to be determined. This information is required for entering the viscous flow calculations.

Viscous Flow

All calculations of the viscous flow are made at one point for both streams: the intersection of the inviscid boundaries. This is because the intersection is on the slipline dividing the two streams; the slip surface is assumed to be the reaction plane upon which the merging streams impinge and divide into the parts which are turned back into the base and those which are recompressed to the downstream pressure. Thus, the properties of the mixing layer positioned at that point are those used for the evaluation of the terms in the primary equations.

The spreading parameter, σ, is calculated from Eq. (42). As this spreading parameter is based on fully developed flow, the elemental species distribution is assumed to follow the velocity profile from the Crocco relation. That is,

$$k = u/U \quad . \tag{79}$$

(A full discussion of the evaluation of a typical integral is provided in the following section.) The axisymmetric correction to σ is applied using either Eq. (58) or

Eq. (59), depending on the assumption of the turbulence level. Equations (17) and (18) can now be solved simultaneously to obtain y_m and C_{mf}. The dividing streamline location, y_D, can then be determined from Eq. (1). The calculations are repeated for each mixing layer.

The equations of the recompression analysis must now be solved iteratively for each mixing layer to determine the location of the stagnating streamlines, y_S. Thus, Eqs. (30), (31), (32), (33), and (34) must be solved together with geometrical relations[1] for X_1 and X_S to determine y_S for each layer.

All the parameters necessary for evaluating the primary equations are now available. The terms are evaluated and the residuals determined. The Newton-Raphson method serves to predict new guesses for p_B, mf_1, and mf_2, and the global iteration proceeds to convergence.

Evaluation of Typical Integral

Consider the integral

$$I_k = \int_{y_L}^{y_S} k\rho u R dy \quad . \tag{80}$$

The local mass fraction of the high-speed stream in the local mixture at a point in the mixing layer is defined by

[1]These relations are as presented in [2] and are easily derived.

Eq. (16). Repeated here, it is

$$k = \frac{1}{2}\left[1 + \text{erf}\left(C_{mf}\frac{\sigma y}{\ell}\right)\right] . \tag{81}$$

The local total enthalpy is

$$H = kH_U + (1 - k)H_B . \tag{82}$$

The velocity at any given y is known from the velocity profile, Eq. (13). Also, the relative moles of each element are determined as

$$N_j = kN_{j\infty} + (1 - k)N_{jB} \quad j=1,m . \tag{83}$$

Since the pressure is known and the static enthalpy is

$$h = H - u^2/2 \tag{84}$$

the mole fractions of the molecular constituents and the temperature are then determined from the equilibrium chemistry; then

$$\rho = \frac{p_B}{t}\left(\frac{\sum_i C_i w_i}{\hat{R}}\right) . \tag{85}$$

The radius to any point in the mixing zone is

$$R = R_i + (y - y_m)\cos\beta . \tag{86}$$

Thus, all elements of the integrand are readily found, and the integration is performed using a conventional quadrature.

CHAPTER IV

RESULTS AND DISCUSSION

I. Introduction

Checking the theory with experimental data began with the classical two-dimensional, backward-facing step problem. Quite a large amount of data exists for this configuration [8]. It served not only as a check on the recompression model, but it provided critical data on the effect of the initial boundary layer.

Davis [33], for his dissertation, performed some interesting experiments by bleeding hydrogen gas into the base region of the backward-facing step and taking measurements both with and without burning. This provided the information to check the effects of both base bleed and chemistry.

There remained only to find data for the configuration of interest; that is, an axisymmetric jet embedded in a blunt-based afterbody. The Reid and Hastings experiments [34] were ideal for this. Their experiments involved exhausting an embedded supersonic jet into a supersonic stream at various jet-to-stream total pressure ratios. These experiments served to check the axisymmetric approximation. And finally, some unpublished data from an AEDC

test [35], although incomplete, provided a comparison with a hot rocket exhausting into a stream of supersonic air.

II. Backward-Facing Step

Isoenergetic Flows

The data as compiled by [4] are presented in Figs. 7, 8, and 9 along with the corresponding predictions of the present theory. It is assumed that the inviscid stream approaching the backstep is uniform and extends without interference to infinity in the direction transverse to the flow.

The axially symmetric approximation was programmed; so the planar problem was simulated by using the embedded nozzle in a blunt-afterbody configuration. The nozzle was extended in radius, in comparison to the height of the base, until the axisymmetric effect was negligible; that is, the ratio of the nozzle radius to the base height was 50:1. The nozzle half-angle was taken as zero, and the conditions on the exit plane made identical to those of the outer flow.

To test the effect of the momentum thickness Reynolds number, the correlation given graphically by [4] was used. It is reproduced in Fig. 10.

The relatively flat trajectory of the theoretical prediction of base pressure with respect to momentum thickness indicated that the recompression model was behaving correctly. The recompression model of [2] was

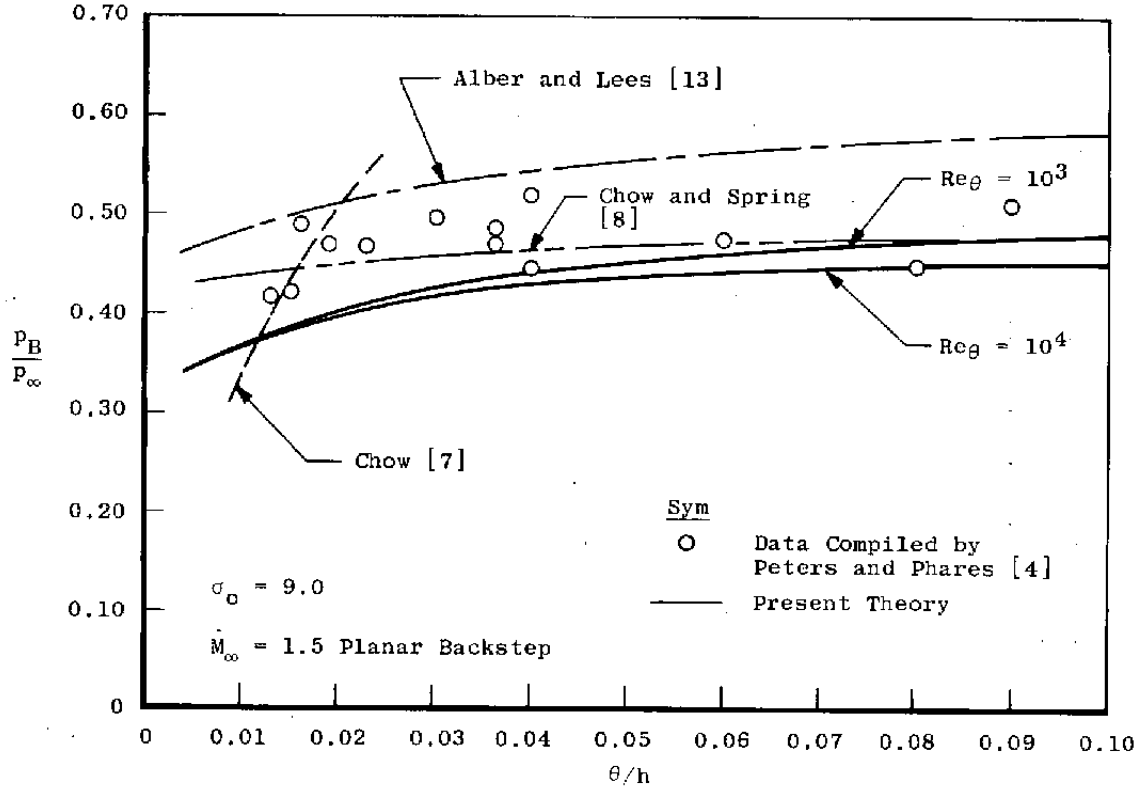

Figure 7. Base pressure vs momentum thickness of initial boundary layer (M_∞ = 1.5).

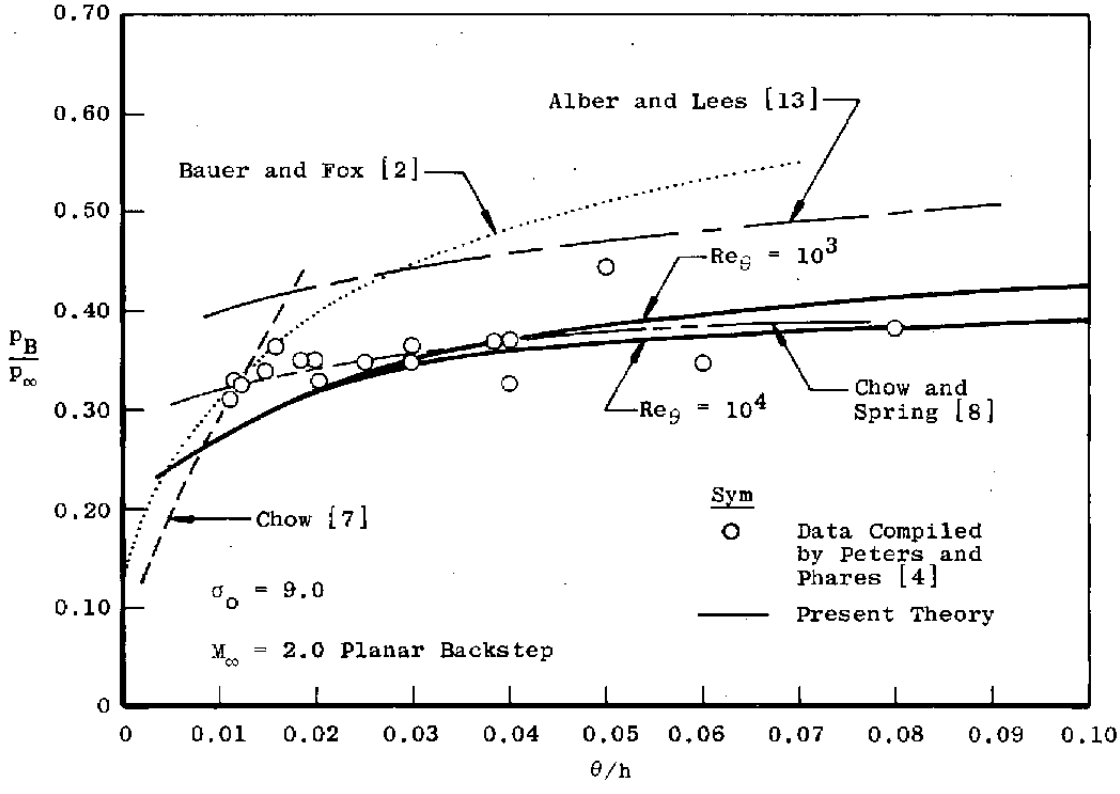

Figure 8. Base pressure vs momentum thickness of initial boundary layer (M_∞ = 2.0).

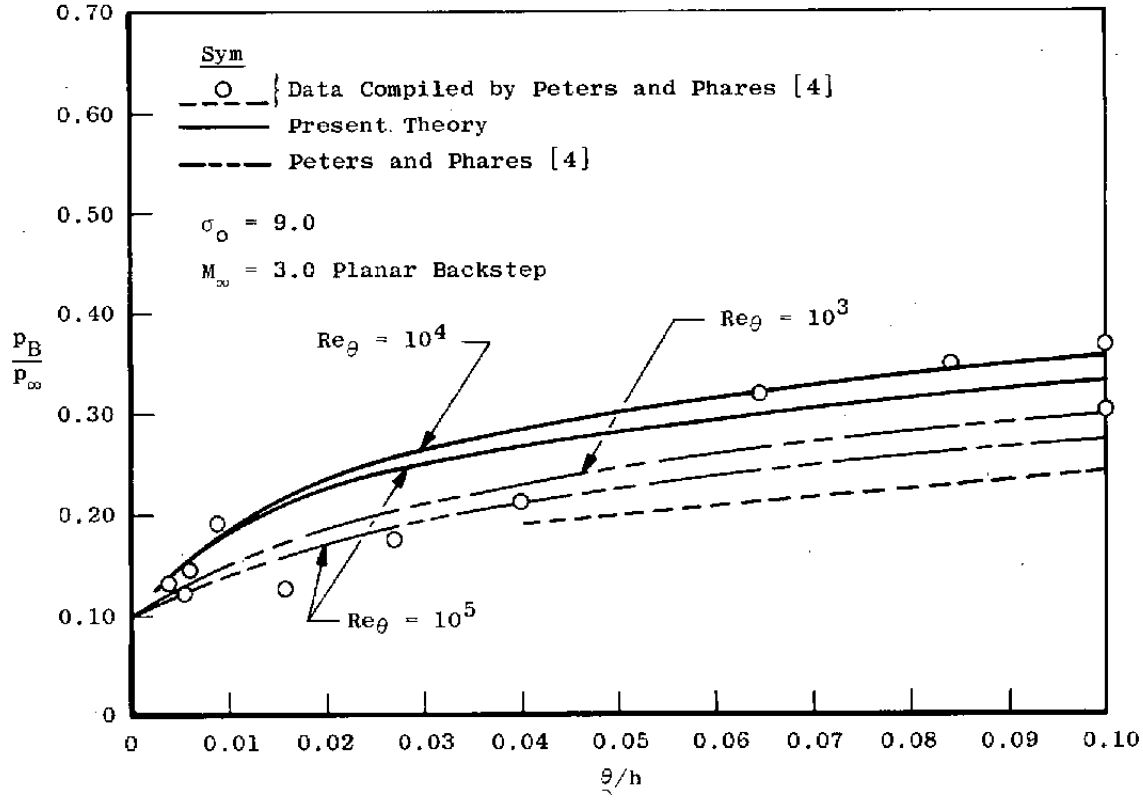

Figure 9. Base pressure vs momentum thickness of initial boundary layer (M_∞ = 3.0).

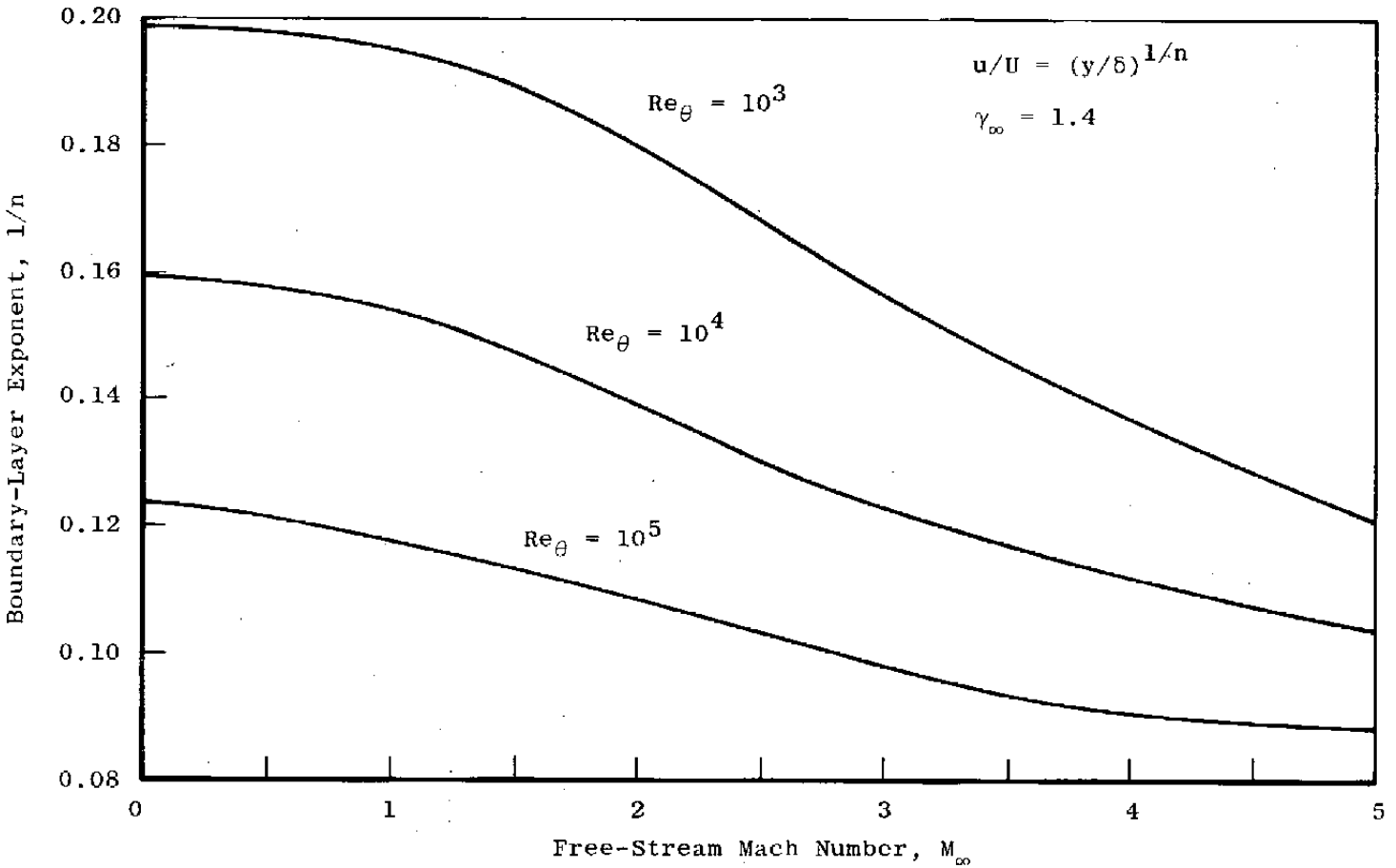

Figure 10. Boundary-layer profile exponent for adiabatic flow along a flat plate from Peters and Phares [4].

based on an inviscid assumption. It is shown for comparison in Fig. 8. Data scatter is typical of these experiments. Part of this is attributed to wall effects, and part is due to the different histories of the flows. (See [15].)

In Fig. 11, the recompression factor of Nash [10] is predicted as a function of the boundary-layer momentum thickness. These recompression-factor curves are those which correspond with the base pressures of Figs. 7, 8, and 9. As Nash did not take into account the initial boundary layer, comparisons are difficult. However, he stated that a recompression factor of 0.35 correlated data well for supersonic Mach numbers. In the present case, say at a Mach number of 2.0, a recompression factor of 0.35 corresponds to a θ/h of about 0.038, which is quite typical.

Perhaps the most severe test of the present theory was afforded by the data [36] presented in Fig. 12. Here, computations were made to boundary-layer thicknesses which were approximately nine times the step height. After approximately a θ/h of 0.8, convergence became very slow; and finally, convergence could not be achieved at all.

At a Mach number of 1.5, Fig. 7, the predictions fall low in the data. However, Fig. 13 compares the predictions with data from Tanner [9]. Although he gives no initial boundary-layer information, it was found that a boundary-layer momentum thickness of 0.04 agreed almost

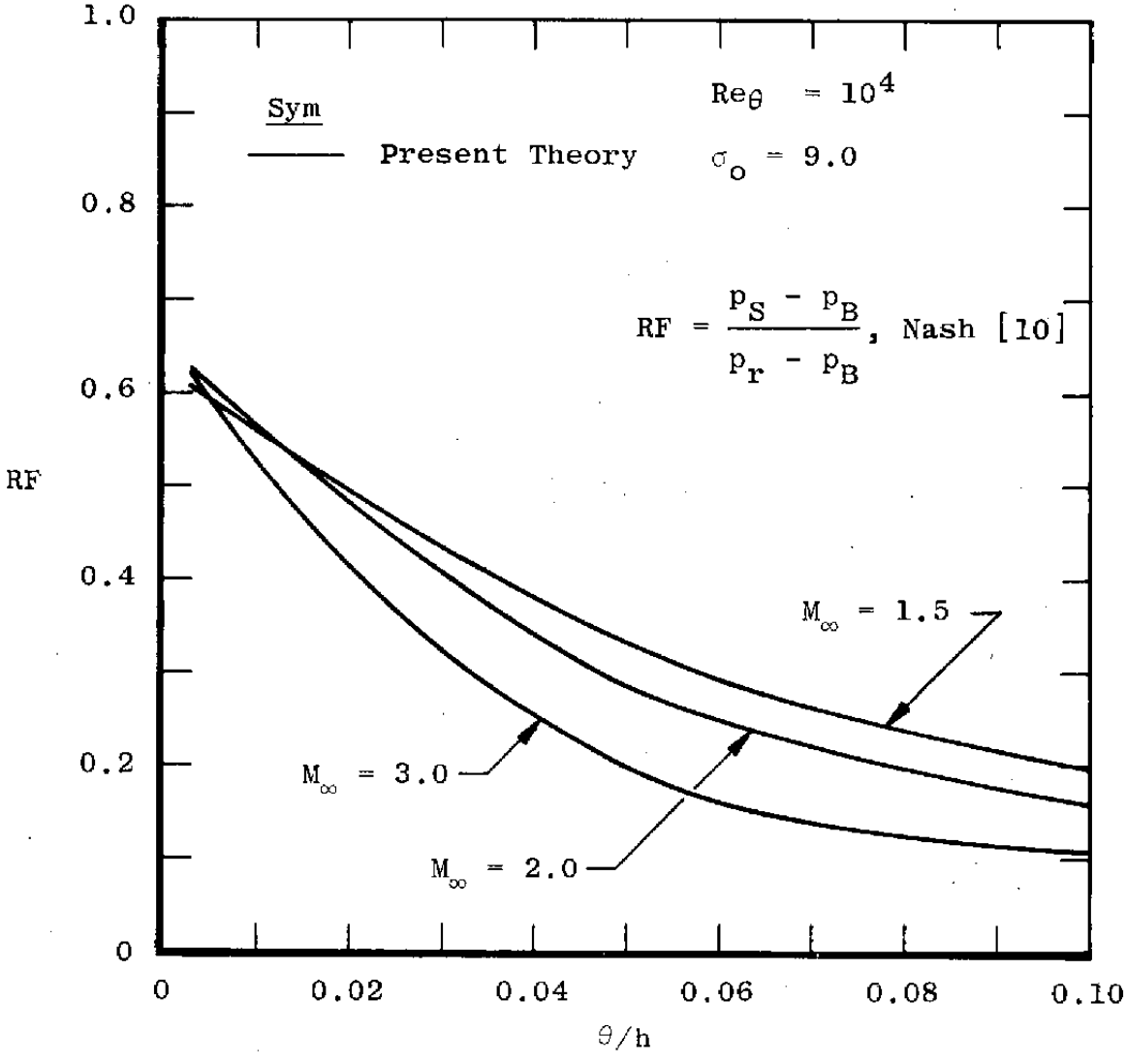

Figure 11. Theoretical prediction of the Nash recompression factor.

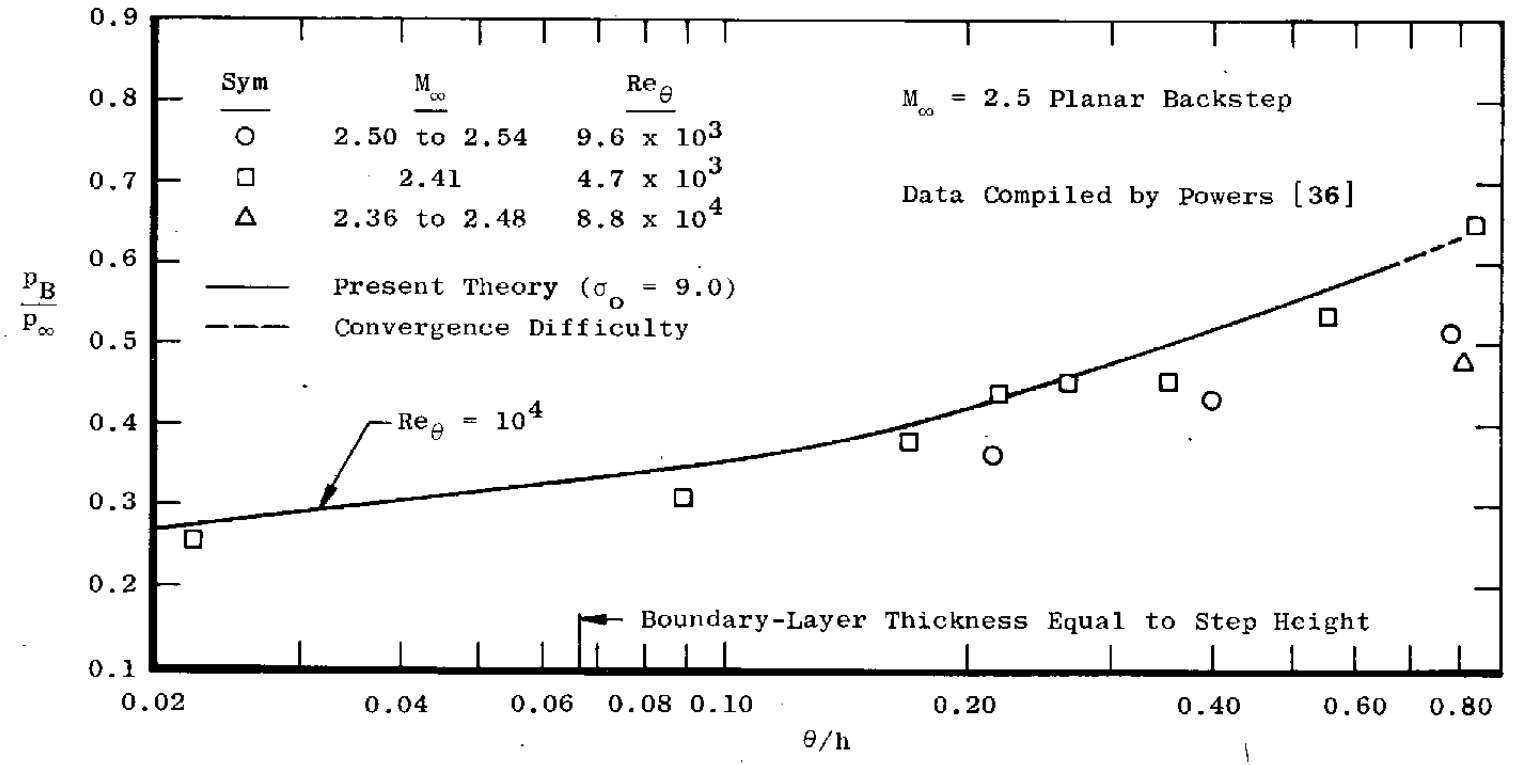

Figure 12. Base-pressure predictions at very large initial boundary-layer momentum thicknesses.

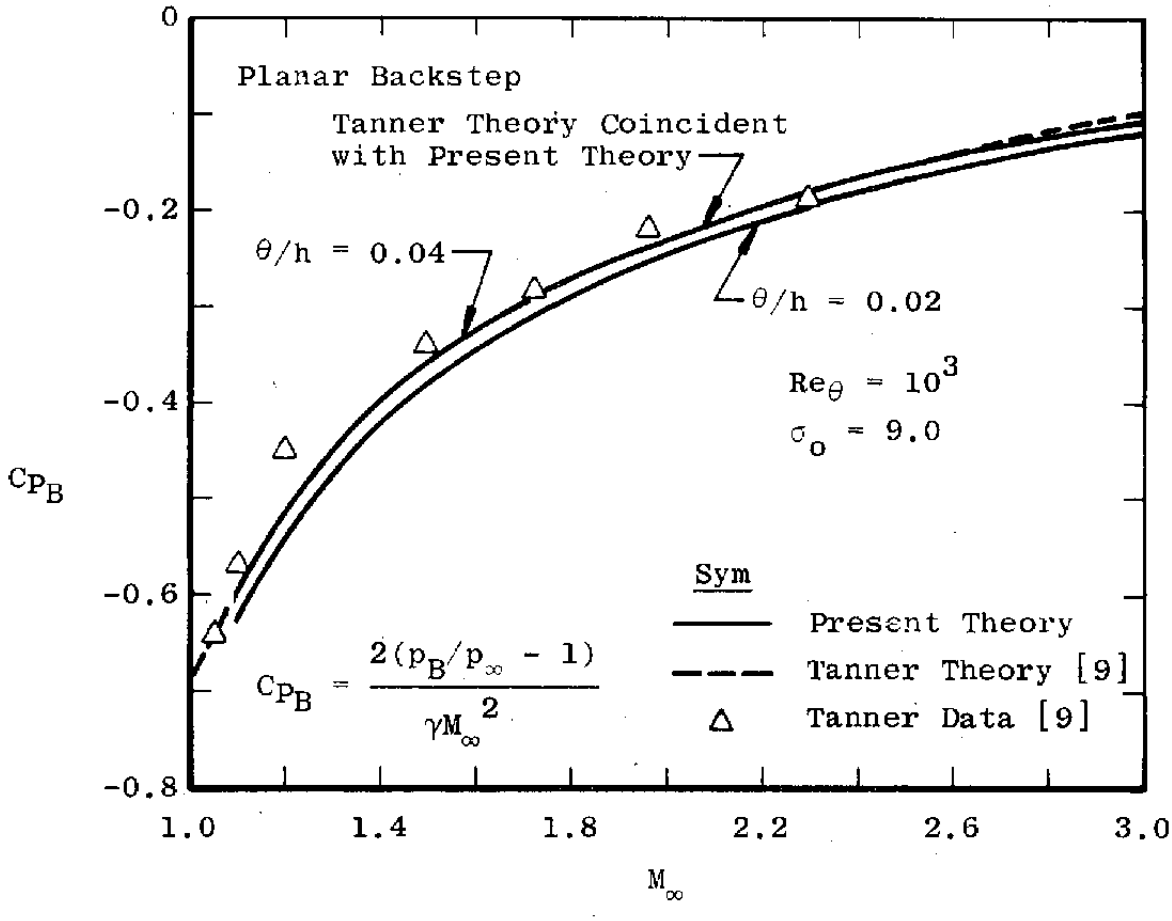

Figure 13. Base-pressure coefficient as a function of Mach number (Tanner's data).

exactly with his theory, which he claims to be a good prediction of base pressures in the low supersonic range.

From these results, it was concluded that the theory worked quite well for cold, planar flows without any base bleed. The next test would be the predicting of base pressures with base bleed and with burning.

Base Bleed and Burning

Davis [33] performed the following experiments. A blunt-based afterbody was immersed in an air stream flowing at a Mach number of 2.0. Hydrogen was bled into the base region at various flow rates. The base-pressure change was plotted against the flow rates producing the lower data curve of Fig. 14. Then, a pilot flame was ignited and the bleed flow was adjusted to the desired rate. The flame was extinguished when the wake burning was self-sustaining. The base temperature and pressure were plotted producing the upper curve of Fig. 14 and the data curve of Fig. 15.

Computations were made to simulate the experiments. The results are plotted with the data curves of Figs. 14 and 15. As Davis obtained no initial boundary-layer data, the boundary-layer thickness of the theory was adjusted until the computed base pressure with no bleed matched the zero bleed flow point of the data. With a σ_o of 12.0, this pressure was obtained at a θ/h value of 0.019. At a σ_o of 9.0, a θ/h value of 0.04 was required. When burning was initiated in the computations at a σ_o of 9.0, no solutions

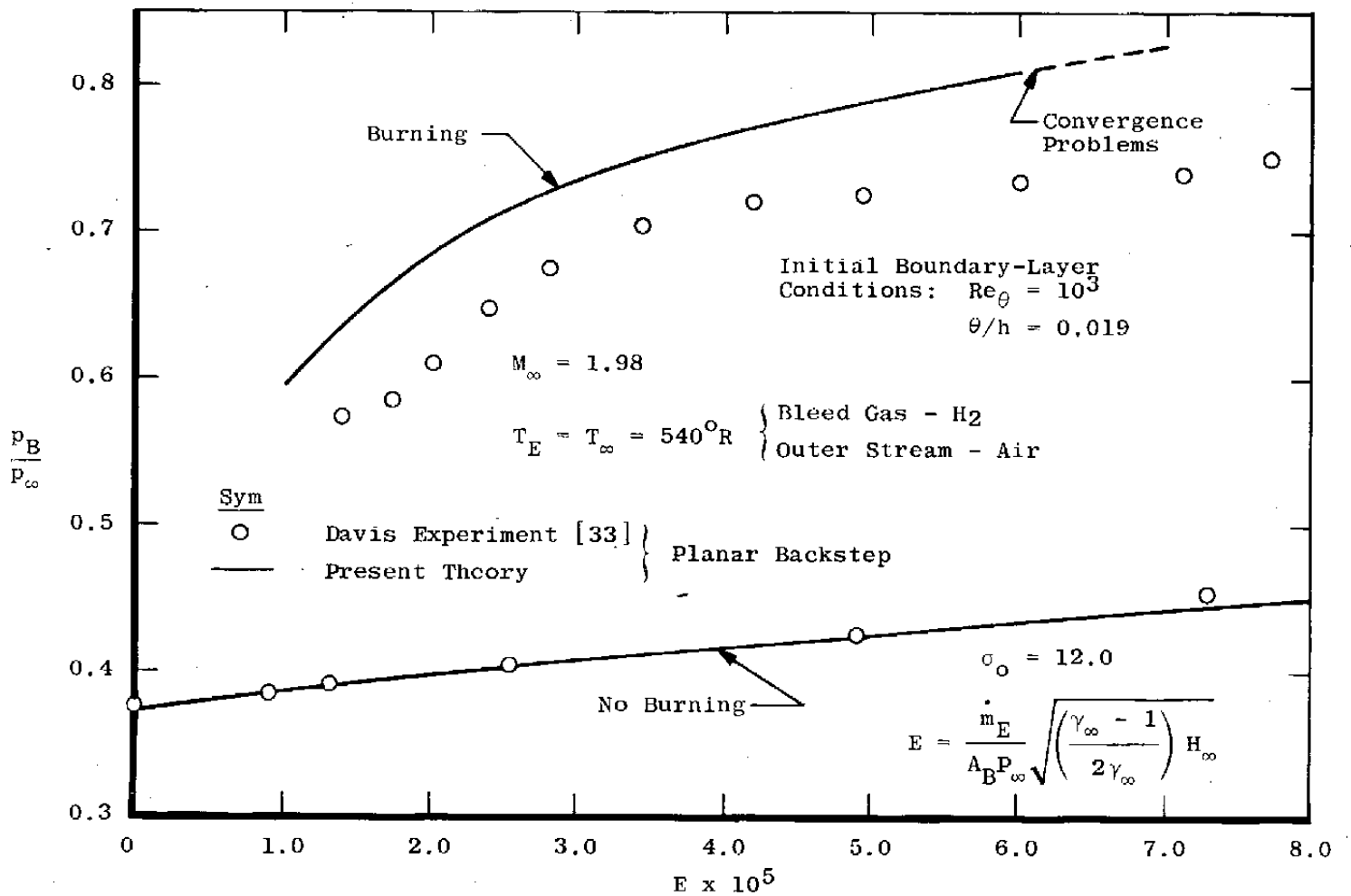

Figure 14. Effect on the base pressure of a hydrogen bleed both with and without burning.

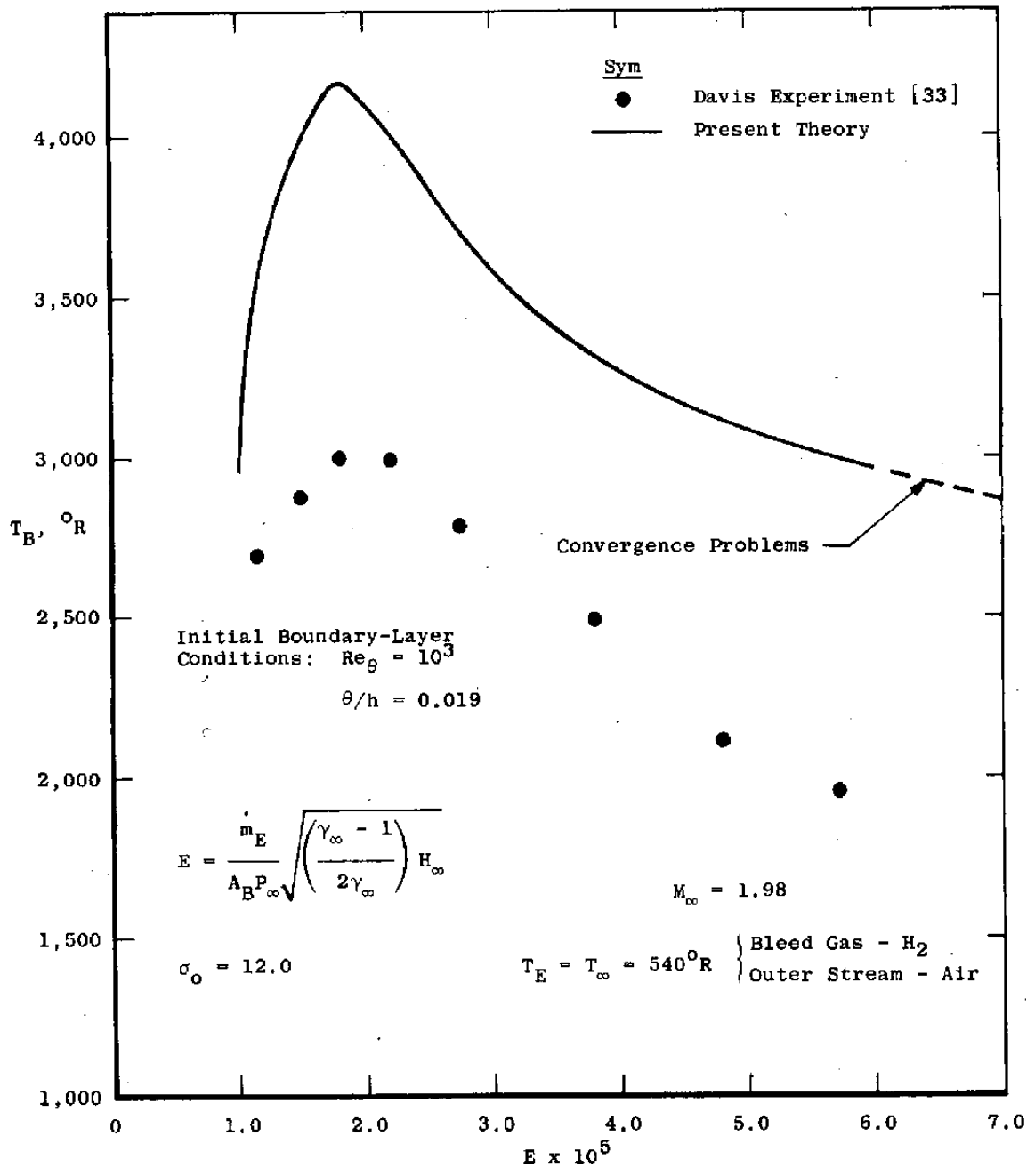

Figure 15. The effect on the base temperature of hydrogen bleed with burning.

were found. The curves presented are those calculated at a σ_o of 12.0. It is not clear that any physical significance can be attached to conditions with a σ_o of 9.0, for even with the computations at a σ_o of 12.0 after a bleed rate parameter, H, of 6.0×10^{-5}, convergence became very slow; and then finally, no convergence could be obtained. Perhaps all that can be reasonably said is that the limits of the theory are being observed and nothing more.

The pressure prediction is high, but acceptable. The temperature prediction is also high; however, the location of the peak is well predicted, which indicates that the basic flow mechanism is well modeled. It is interesting to observe that in Davis' theoretical approach, he input the base pressure as knowns to obtain the base temperatures. As pointed out in Chapter II, Section VII, his flame-sheet model disallows oxidizer in the base region, which accounts for his lower temperature predictions, for the peak temperatures in the mixing layer of approximately 4300°R are predicted by his method, which matches the peak temperatures of the present theory. That is, if oxidizer is in the base, at some bleed rate stoichiometric conditions must occur. It is perhaps also worthy of note that the adiabatic equilibrium conditions as assumed by the theory are rarely achievable in real experiments of this type due to the effects of wall cooling, thermocouple errors, and combustion inefficiency.

The curves of Fig. 16 are presented to show temperature profiles as predicted by the theory. No data are presented as Davis' recordings across the mixing layer were too sparse to encompass this area.

In conclusion, here, it must be said that the predicted shapes of the curves, particularly the base pressure curves, show that the basic physics of this configuration is well predicted; the theory requires only a more realistic chemistry model.

III. Correction for Axially Symmetric Effects

As previously pointed out, the theory is two-dimensional. However, the corrections for axisymmetric effects were employed as detailed in Chapter II, Section X. Reid and Hastings [34] recorded the effect of total pressure ratio as between the embedded jet and the external stream, both of which were at a Mach number of 2.0. Complete initial boundary-layer information was provided which allowed the best check yet of the present theoretical approach. For the configuration where the outside radius is of a ratio of 1.67 to the nozzle radius, the following information was provided:

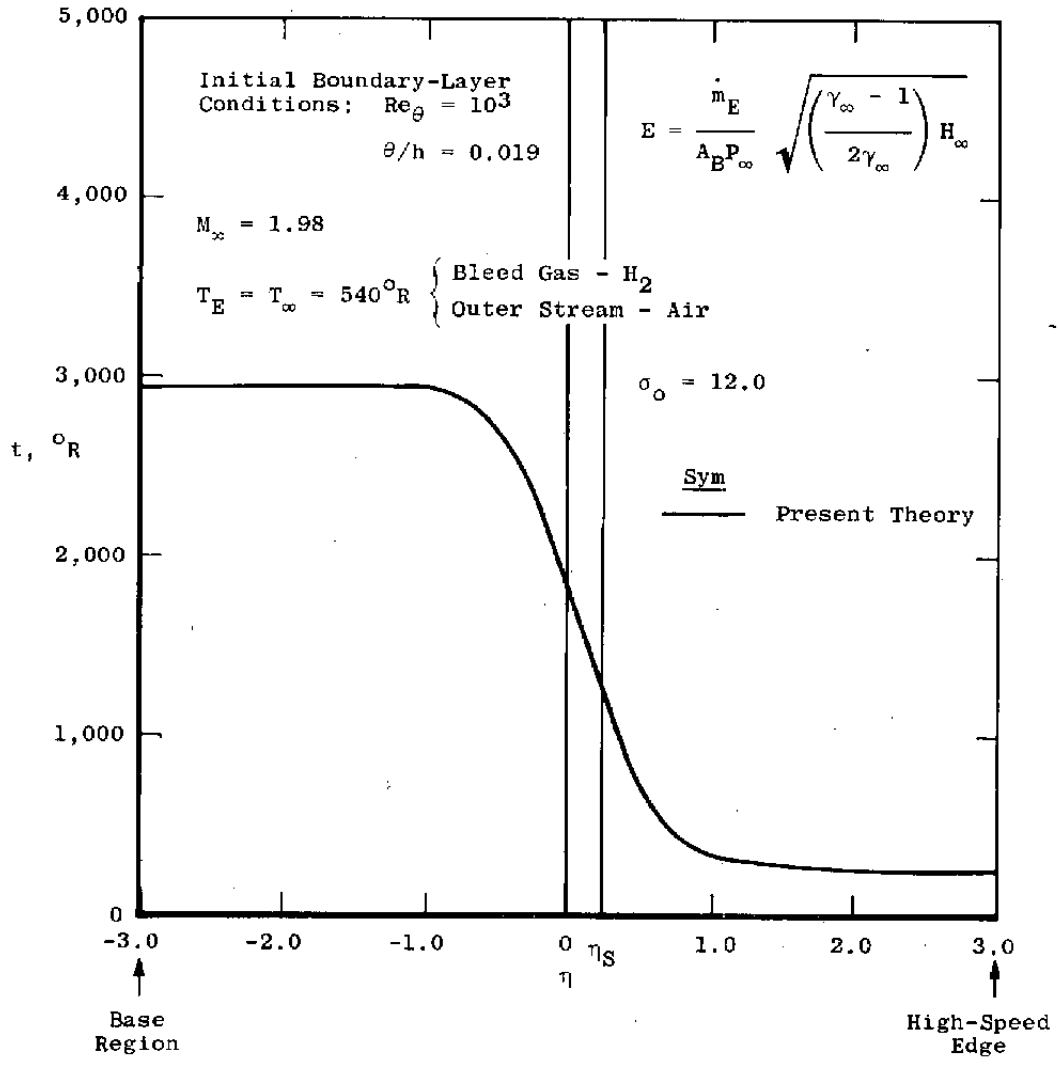

a. $E = 1 \times 10^{-5}$

Figure 16. Static temperature distribution across mixing layers as predicted by theory.

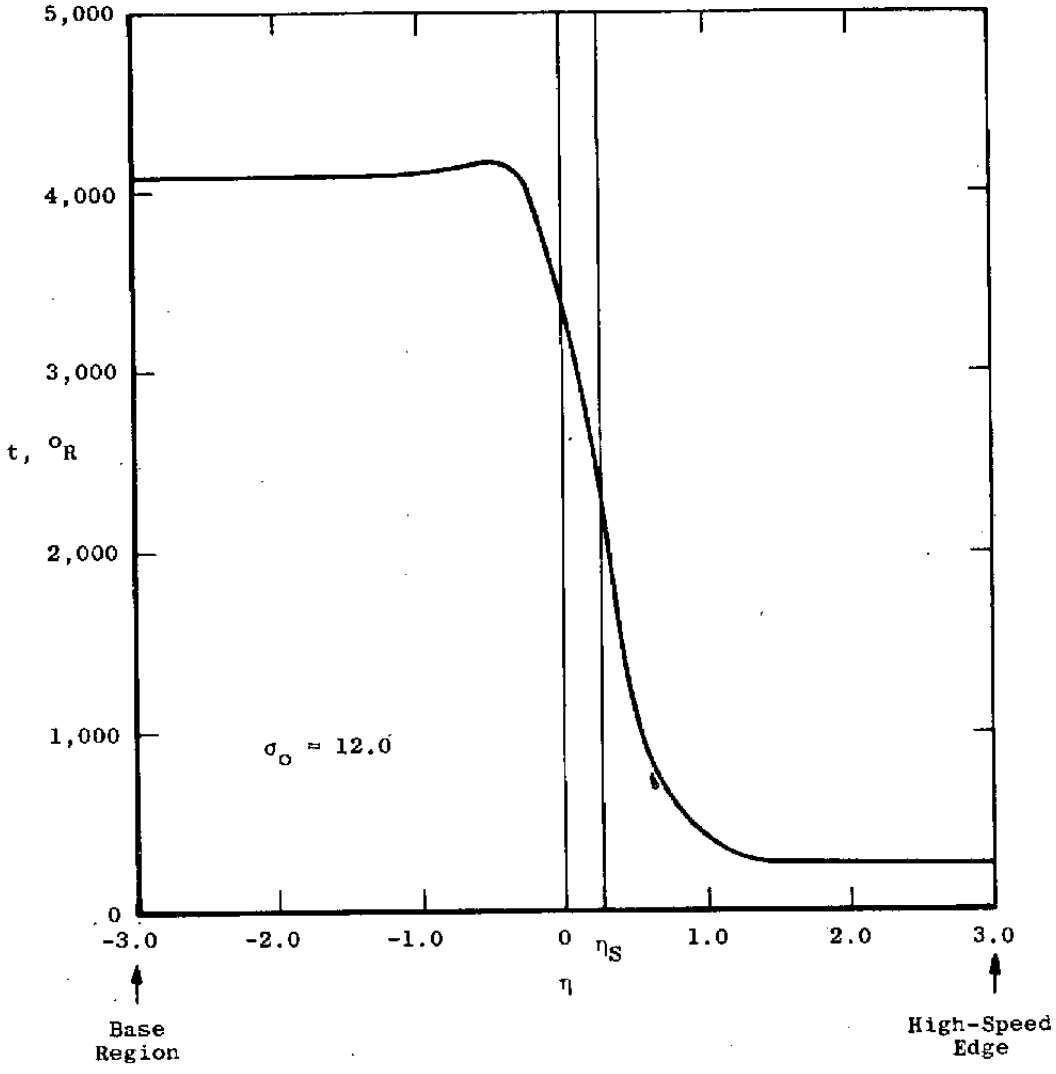

b. $E = 1.5 \times 10^{-5}$

Figure 16. (Continued)

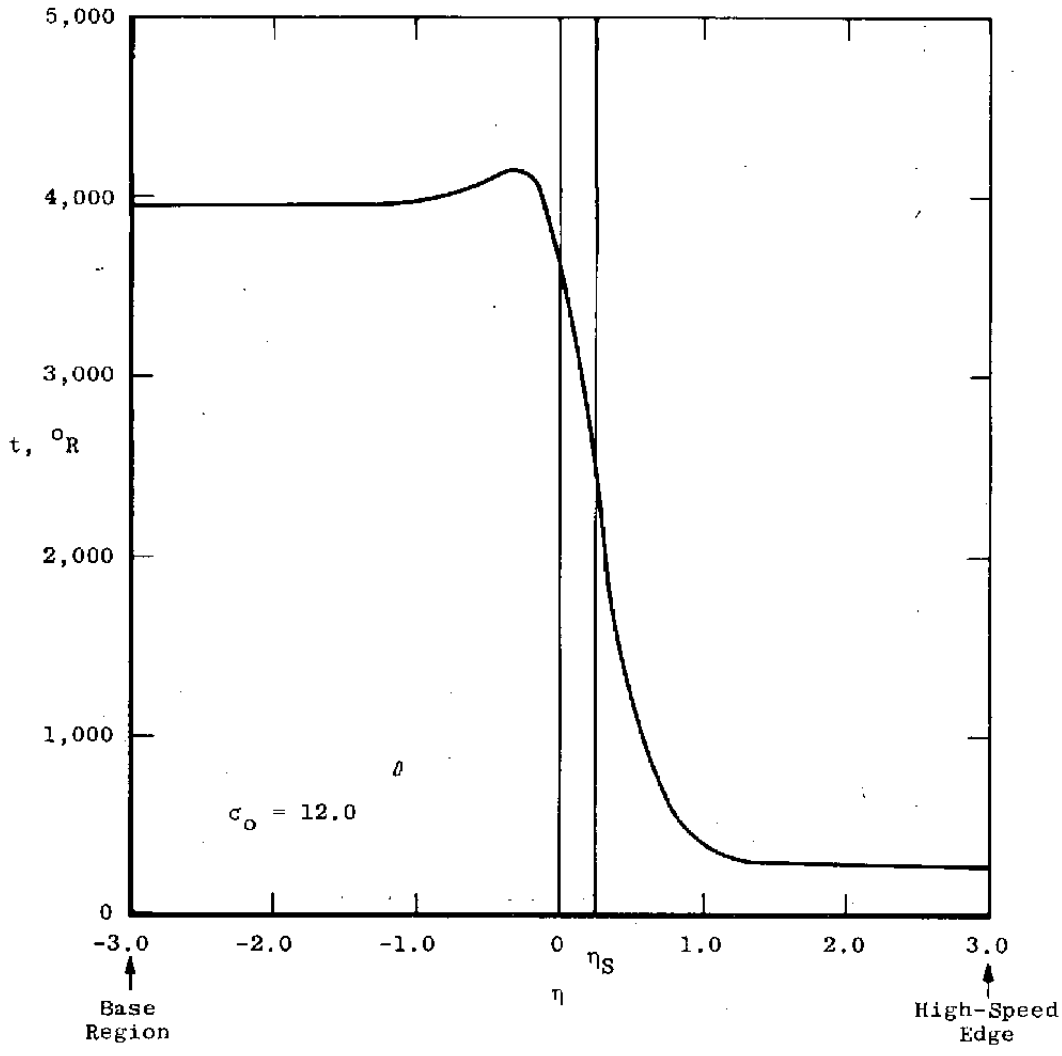

c. E = 2.25 x 10^{-5}

Figure 16. (Continued)

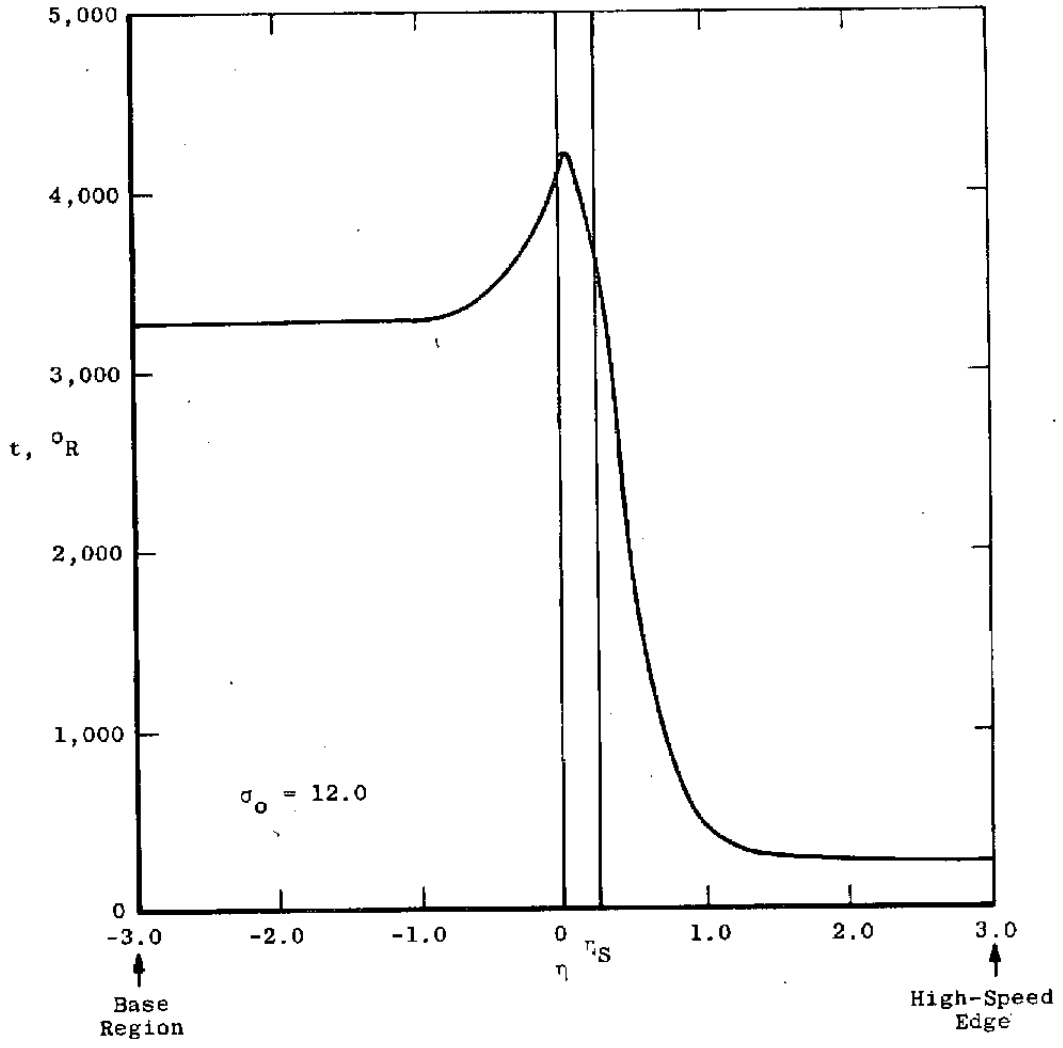

d. $E = 4.0 \times 10^{-5}$

Figure 16. (Continued)

Nozzle

$R_1 = 1.17$ in.,

$\theta_1 = 0.0037$ in.,

$\frac{\delta_1^*}{\theta_1} = 2.78$ in the base plane.

External Body

$R_2 = 1.95$ in.,

$\theta_2 = 0.0165$ in.,

$\frac{\delta_2^*}{\theta_2} = 2.97$ in the base plane.

A power law exponent of 1/9 and boundary-layer thicknesses, $\delta_1/R_1 = 0.048$ and $\delta_2/R_1 = 0.212$, gave the correct momentum thicknesses. Boundary-layer information was not given on the other nozzles; but since the aspect ratios of the nozzles were approximately equal, the value of 0.048 for δ_1/R_1 was used for the others as well. The external momentum thicknesses were the same for all configurations.

Using an incompressible reference spreading parameter, σ_o, of 9.0, and a σ_A as derived in Chapter II, Section X, the results presented in Fig. 17 were obtained.

The prediction at R_2/R_1 equal to 1.25 was particularly welcomed as it further confirmed the basic theory as this case is close to being two-dimensional. As the radius

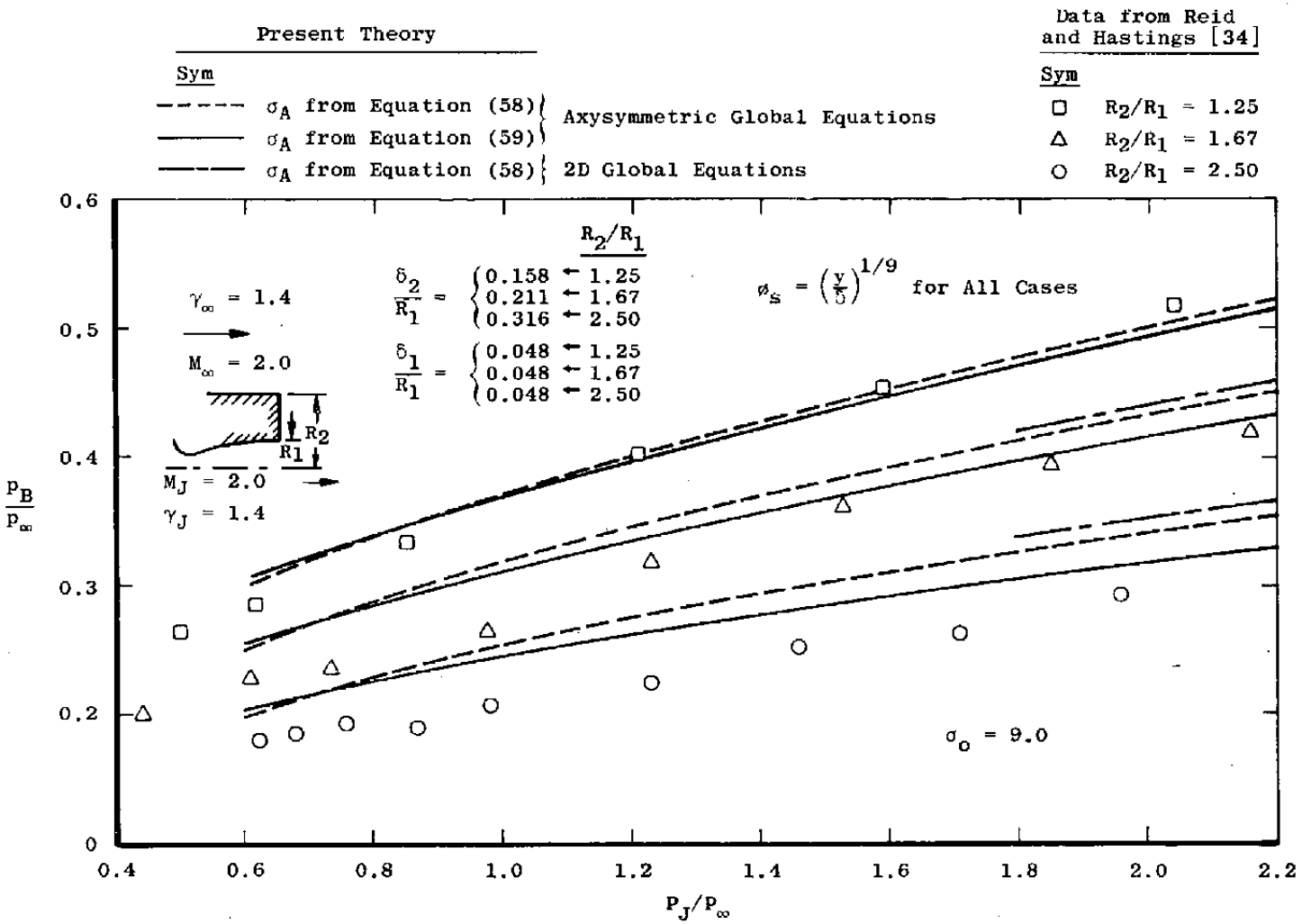

Figure 17. Relationship between base pressure and the jet-to-free-stream total pressure ratio of axially symmetric jet.

ratio is increased and the axisymmetric effects become more apparent, the approximation is not quite as good, but still acceptable. For these cases, the conventional Mangler transformation which produces the spreading parameter of Eq. (59) gives the best results; however, the σ_A of Eq. (59) appears to better follow the shape of the data curve.

The last axisymmetric configuration attempted was at once the most complex and the most incomplete. Its complexity stems from the fact that it is a hot-rocket exhaust (γ = 1.26) embedded in a relatively large base submerged in a supersonic air stream. It is incomplete because the initial boundary layer is defined only by its thickness, and the base pressure is the only parameter that was measured. Nevertheless, a series of runs was made at external stream Mach numbers of 2.05 and 3.00, the results of which are shown in Fig. 18.

The external boundary-layer thickness was maintained at 67 percent of the nozzle radius, and the different momentum thicknesses resulted from varying the shape of the profile. The results at the lower Mach number are reasonable although a relatively large momentum thickness is required to match the recorded base pressure. In all cases the boundary-layer momentum thickness of the jet was maintained at approximately 2 percent of the base thickness.

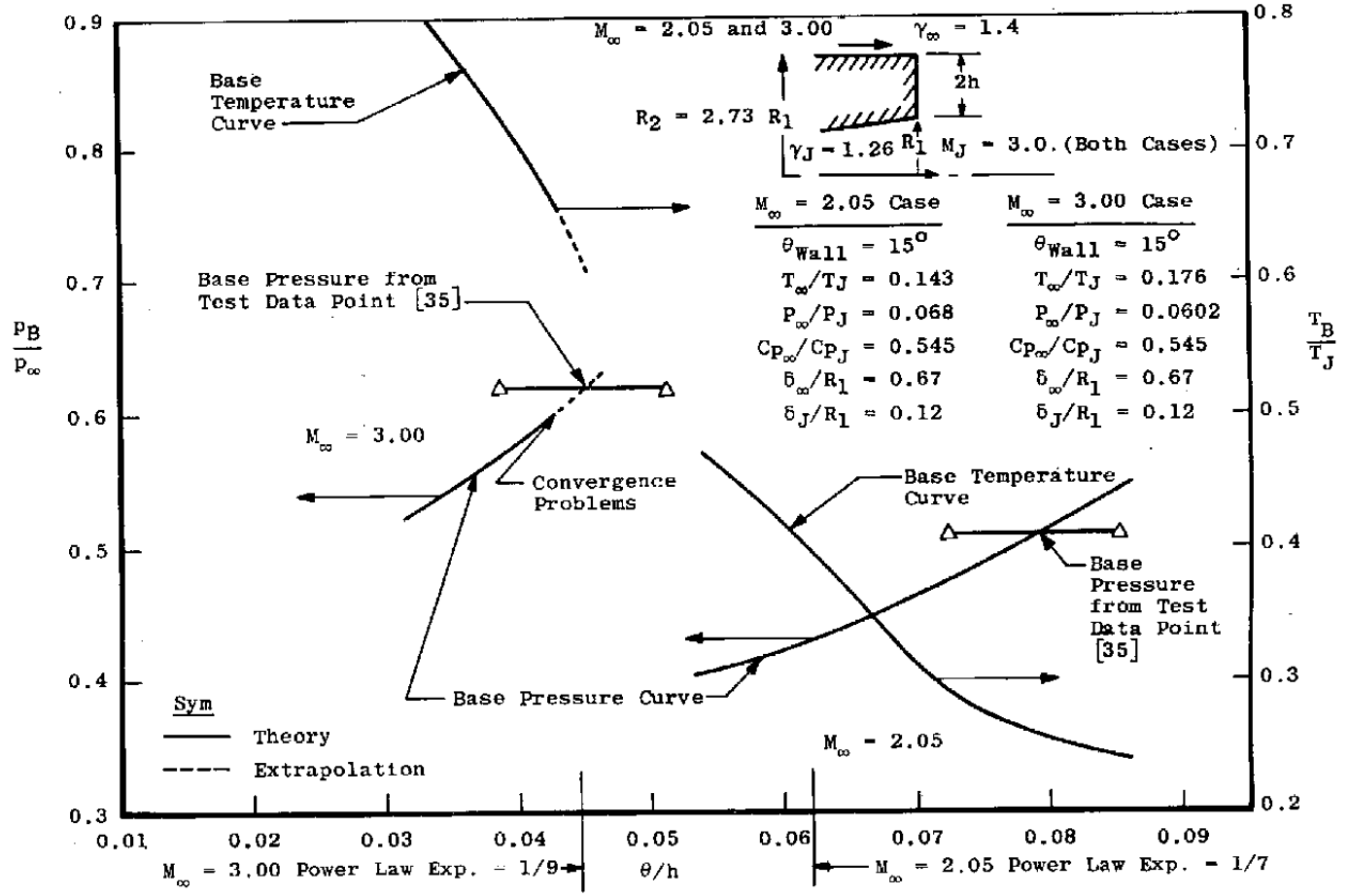

Figure 18. Calculated base temperatures and pressures for a hot rocket at two external stream Mach numbers with varying external boundary-layer momentum thicknesses.

The results at the higher Mach number were disappointing in that near the recorded base pressure convergence was not achieved. What is apparent, however, is the effect of the external boundary layer on the temperature and pressure of the base.

In both Mach number cases, the temperature drops with increasing external boundary-layer momentum thickness. This is because more of the external stream and less of the rocket exhaust are captured in the base region. Because of the much larger thickness of the outer boundary layer, however, it tends to be the overriding mechanism affecting the base pressure.

All calculations for this case were made assuming frozen chemistry as equilibrium chemistry results were quite unrealistic. They indicated that burning was occurring, which served to drive pressures and temperatures much higher than experiment would indicate.

CHAPTER V

CONCLUSIONS AND RECOMMENDATIONS

A generalized supersonic base-flow theory has been developed for the near-wake region behind bluff-based, two-dimensional and axially symmetric bodies in the presence of a coaxial, supersonic jet. The theory works well.

The correlations presented show the theory to be viable and physically realistic. In particular, a new recompression model was able to generalize the mixing analysis and extend the overall theory to encompass many complex and diverse flow configurations, including those with very thick boundary layers. The new species distribution model allowed flows with hydrogen bleed to be predicted as well as flows with large total temperature differences between the base and the high-speed streams. As the mechanism was available, a chemical equilibrium analysis was coupled to the theory. It gave an excellent prediction of the point at which the base bleed rate would produce the maximum base temperature. It also gave a good prediction of the effect of burning on the base pressure.

The Mangler transformation was used to develop an axially symmetric correction to the two-dimensional spreading parameter for highly turbulent mixing. The transformation also was used to provide an axisymmetric correction to the spreading parameter for low-turbulence

and laminar flows. However, interesting and useful as these corrections were, they further amplified an underlying problem: the lack of a good model for the spreading parameter.

Indeed, perhaps the most important result of this investigation was the realization that the modeling of the spreading parameter needs further development. There is a tendency in the literature to treat the spreading parameter as an off-the-shelf item, important only to the extent that some numerical value must be chosen. This is understandable, of course, when the heavy hand of empiricism must be used to nudge an unsatisfactory solution into the area of reality, as is necessary when a recompression factor is used, and the initial boundary layer is ignored. However, as the basic theory becomes more realistic and inclusive, the necessity of a more realistic spreading parameter becomes apparent. Specifically, the spreading parameter must mimic reality to the extent that it develops as the mixing develops and is asymptotic to the fully developed value, taking into account the history of the separating boundary layers.

Although turbulent flows were of primary interest in the present analysis, appropriate modeling of the spreading parameter would allow the theory to be extended to laminar mixing. This becomes important in low-density flows.

Perhaps the weakest point in the present theory is the lack of a good model for axially symmetric mixing. The assumption of planar mixing, while giving acceptable predictions for the most part, did begin to fail at afterbody-to-nozzle radius ratios greater than 1.67.

Again, in overview, it must be said that the present theory works well. It predicted the effect of the initial boundary layer in planar flow as well or better than more sophisticated analyses up to very high momentum thicknesses. The theory predicted well the effect of hydrogen bleed both with and without burning. Predictions of axially symmetric flows with coaxial cold jets were excellent for small bases and quite acceptable for the larger bases. It is concluded that the present theory is at least the equal of the Crocco-Lees approach to simple flows, and it is superior when applied to complex flows such as the two-mixing-layer problem.

The extension to flows with nonequilibrium chemistry should be a fertile ground for further work. By coupling a rate equation to the system and adding the nonequilibrium term to the thermodynamic property relations, the present theory should be able to predict the effect of nonequilibrium on the near wake.

BIBLIOGRAPHY

1. Korst, H. H., W. L. Chow, and G. W. Zumwalt. "Research on Transonic and Supersonic Flow of a Real Fluid at Abrupt Increases in Cross Section--Final Report," ME Technical Report 392-5, University of Illinois, Urbana, December, 1959.

2. Bauer, R. C., and J. H. Fox. "An Application of the Chapman-Korst Theory to Supersonic Nozzle-Afterbody Flows," Arnold Engineering Development Center TR-76-158, Arnold Air Force Station, Tennessee, January, 1977.

3. Crocco, L., and L. Lees. "A Mixing Theory for the Interaction Between Dissipative Flows and Nearly Isentropic Streams," Journal of the Aeronautical Sciences, 19:649-676, October, 1952.

4. Peters, C. E., and W. J. Phares. "Analytical Model of Supersonic, Turbulent, Near-Wake Flows," Arnold Engineering Development Center TR-76-127, Arnold Air Force Station, Tennessee, September, 1976.

5. Murthy, S. N. B., and J. R. Osborn. "Base Flow Phenomena with and without Injection: Experimental Results, Theories, and Bibliography," Progress in Astronautics and Aeronautics, S. N. B. Murthy, et al., editors. Vol. 40. Cambridge, Massachusetts: The MIT Press, 1976. Pp. 7-210.

6. Yaros, S. F. "An Analysis of Transonic Viscous/Inviscid Interactions on Axisymmetric Bodies with Solid Stings or Real Plumes." Ph.D. dissertation, The University of Tennessee, Knoxville, 1977.

7. Chow, W. L. "Recompression of a Two-Dimensional Supersonic Turbulent Free Shear Layer," Proceedings of the Twelfth Midwestern Mechanics Conference, L. H. N. Lee, et al., editors. Vol. 6. Notre Dame: University of Notre Dame Press, 1971. Pp. 319-332.

8. Chow, W. L., and D. J. Spring. "Viscous Interaction of Flow Redevelopment After Flow Reattachment with Supersonic External Stream," AIAA Journal, 13(No. 12):1576-1584, December, 1975.

9. Tanner, M. "Two Different Theoretical Approaches to the Base Pressure Problem in Two-Dimensional Supersonic Flow," The Aeronautical Quarterly, 29:114-130, May, 1978.

10. Nash, J. F. "An Analysis of Two-Dimensional Turbulent Base Flow, Including the Effect of the Approaching Boundary Layer," Ames Research Center R&M 3344, Ames, California, July, 1962.

11. Addy, A. L. "Analysis of the Axisymmetric Base-Pressure and Base-Temperature Problem with Supersonic Interacting Free Stream-Nozzle Flows--Based on the Flow Model of Korst, et al.--Part I," U. S. Army Missile Command RD-TR-69-12, Redstone Arsenal, Alabama, July, 1969.

12. Page, R. H., F. J. Kessler, and W. G. Hill, Jr. "Reattachment of Two-Dimensional Supersonic Turbulent Flows." ASME Paper No. 67-FE-20, ASME Fluids Engineering Conference, Chicago, Illinois, August, 1967.

13. Alber, I. E., and Lester Lees. "Integral Theory for Supersonic Turbulent Base Flows," AIAA Journal, 6(No. 7):1343-1355, July, 1968.

14. Strahle, W. C., and G. Mehta. "Turbulent Axisymmetric Base Flow Studies for External Burning Propulsion," Eleventh JANNAF Combustion Meeting. Vol. 2. Silver Spring: Chemical Propulsion Information Agency, 1974. Pp. 441-448.

15. Hussain, A. K. M. F., and M. F. Zedan. "Effect of the Initial Condition on the Axisymmetric Free Shear Layer: Effects of the Initial Momentum Thickness," Physics of Fluids, 21(No. 7):1100-1112, July, 1978.

16. Rhudy, J. P., and J. D. Magnan, Jr. "Turbulent Cavity Flow Investigation at Mach Numbers 4 and 8," Arnold Engineering Development Center TR-66-73, Arnold Air Force Station, Tennessee, June, 1966.

17. Chapman, A. J., and H. H. Korst. "Free Jet Boundary with Consideration of Initial Boundary Layer," Proceedings of the Second U. S. National Congress of Applied Mechanics. New York: The American Society of Mechanical Engineers, 1954. Pp. 723-731.

18. Forsythe, G. E., and W. R. Wasaw. Finite-Difference Methods for Partial Differential Equations. New York: John Wiley and Sons, Inc., 1960.

19. Davis, L. R. "Experimental and Theoretical Determination of Flow Properties in a Reacting Near Wake," AIAA Journal, 6(No. 5):843-847, May, 1968.

20. McBride, B. J., Sheldon Heimel, Janet G. Ehlers, and Sanford Gordon. "Thermodynamic Properties to 6000°K for 210 Substances Involving the First 18 Elements," NASA SP-3001, Washington, D. C., October, 1963.

21. Vincenti, Walter G., and Charles H. Kruger, Jr. Introduction to Physical Gasdynamics. New York: John Wiley and Sons, Inc., 1965.

22. Abramovich, G. N. The Theory of Turbulent Jets, ed. Leon H. Shindel. Cambridge, Massachusetts: The MIT Press, 1963.

23. Libby, P. A. "Theoretical Analysis of Mixing of Reactive Gases with Application to Supersonic Combustion of Hydrogen," Journal of the American Rocket Society, 32(No. 3):388-396, March, 1962.

24. Korst, H. H., and W. Tripp. "The Pressure on a Blunt Trailing Edge Separating Two Supersonic, Two-Dimensional Air Streams of Different Mach Numbers and Stagnation Pressures but Identical Stagnation Temperatures," Fifth Midwestern Conference on Fluid Mechanics. Ann Arbor: University of Michigan Press, 1957. Pp. 187-199.

25. Channapragada, R. S. "Compressible Jet Spread Parameter for Mixing Zone Analysis," AIAA Journal, 1(No. 9):2188-2189, September, 1963.

26. Bauer, R. C. "An Analysis of Two-Dimensional Laminar and Turbulent Compressible Mixing," AIAA Journal, 4(No. 3):392-395, March, 1966.

27. Birch, S. F., and J. M. Eggers. "A Critical Review of the Experimental Data for Developed Free Turbulent Shear Layers," NASA SP-321, Washington, D. C., January, 1973.

28. Bauer, R. C. "Characteristics of Axisymmetric and Two-Dimensional Laminar Boundary Layers," Arnold Engineering Development Center TR-63-253, Arnold Air Force Station, Tennessee, December, 1963.

29. Tetervin, N. "A Generalization to Turbulent Boundary Layers of Mangler's Transformation Between Axisymmetric and Two-Dimensional Laminar Boundary Layers," U. S. Naval Ordnance Laboratory NOLTR 69-47, White Oak, Maryland, June, 1969.

30. Dixon, R. J., J. M. Richardson, and R. H. Page. "Turbulent Base Flow on an Axisymmetric Body with a Single Exhaust Jet," AIAA Journal, 7(No. 7):848-853, July, 1970.

31. Fox, J. H. "Axially Symmetric, Inviscid, Real Gas, Non-Isoenergetic Flow Solution by the Method of Characteristics," Arnold Engineering Development Center TR-69-184, Arnold Air Force Station, Tennessee, January, 1970.

32. Dorn, W. S., and D. D. McCracken. Numerical Methods with FORTRAN IV Case Studies. New York: John Wiley and Sons, Inc., 1972.

33. Davis, L. R. "The Effect of Chemical Reactions in the Turbulent Mixing Component on the Dynamics and Thermodynamics of Wake Flow Fields." Ph.D. dissertation, University of Illinois, Urbana, 1964.

34. Reid, J., and R. C. Hastings. "The Effect of a Central Jet on the Base Pressure of a Cylindrical After-Body in a Supersonic Stream," Aeronautical Research Council Reports and Memoranda No. 3224, Ministry of Aviation, London, U. K., 1961.

35. Chriss, D. Private correspondence. Arnold Engineering Development Center, Arnold Air Force Station, Tennessee, September, 1977.

36. Powers, S. G. "Flight-Measured Pressure Characteristics of Aft-Facing Steps in High Reynolds Number Flow at Mach Numbers of 2.20, 2.50 and 2.80 and Comparison with Other Data," NASA TM-72855, Washington, D. C., May, 1978.

37. Weinberg, F. J. "Explicit Equations for the Calculation, by Successive Approximations, of Equilibrium Gas Compositions at High Temperatures: The Hydrogen + Carbon + Oxygen and the Hydrogen + Carbon + Oxygen + Nitrogen Systems without Solid Carbon Formation," Proceedings of the Royal Society of London, 241(Series A):132-140, September, 1957.

38. Osgerby, I. T., and R. P. Rhodes. "An Efficient Numerical Method for the Calculation of Chemical Equilibrium in the H/C/O/N/A System," Arnold Engineering Development Center TR-71-256, Arnold Air Force Station, Tennessee, April, 1972.

APPENDIX A

DETERMINATION OF EQUILIBRIUM GAS COMPOSITION BY SUCCESSIVE APPROXIMATIONS

It is the purpose here to show by example the method of Weinberg [37] as developed by Osgerby and Rhodes [38] to determine the equilibrium gas composition (mole fractions) of a mixture as a function of pressure, temperature, and the relative number of the various elements present.

The C,H,O case is used to illustrate the method. The equilibria are

$$
\begin{aligned}
&CO_2 \overset{\leftarrow}{\rightarrow} CO + \tfrac{1}{2} O_2 \ , \\
&H_2O \overset{\leftarrow}{\rightarrow} H_2 + \tfrac{1}{2} O_2 \ , \\
&H_2O \overset{\leftarrow}{\rightarrow} \tfrac{1}{2} H_2 + OH \ , \\
&\tfrac{1}{2} H_2 \overset{\rightarrow}{\leftarrow} H \ , \\
&\tfrac{1}{2} O_2 \overset{\leftarrow}{\rightarrow} O \ ,
\end{aligned}
\tag{A.1}
$$

and the atom conservation equations are

$$
\begin{aligned}
P_O &= 2p_{CO_2} + p_{CO} + p_{H_2O} + 2p_{O_2} + p_{OH} + p_O \ , \\
P_H &= 2p_{H_2O} + 2p_{H_2} + p_{OH} + p_H \ , \\
P_C &= p_{CO_2} + p_{CO} \ ,
\end{aligned}
\tag{A.2}
$$

where P is the fictitious pressure of the particular element.

The conservation equations are rewritten to eliminate the fictitious pressures by using the fact that

$$\frac{P_H}{P_C} = \frac{N_H}{N_C} = H^r C \ , \tag{A.3}$$

$$\frac{P_O}{P_C} = \frac{N_O}{N_C} = O^r C \ , \tag{A.4}$$

and

$$P_{CO_2} + P_{CO} + P_{H_2O} + P_{O_2} + P_{OH} + P_O + P_{H_2} + P_H = P \ . \tag{A.5}$$

The new conservation relations are, then,

$$F = 2P_{CO_2} + P_{CO} + P_{H_2O} + 2P_{O_2} + P_{OH} + P_O - O^r_C (P_{CO_2} + P_{CO}) = 0 \ , \tag{A.6}$$

$$G = 2P_{H_2O} + 2P_{H_2} + P_{OH} + P_H - H^r_C (P_{CO_2} + P_{CO}) = 0 \ , \tag{A.7}$$

and

$$L = P_{CO_2} + P_{CO} + P_{H_2O} + P_{O_2} + P_{OH} + P_O + P_{H_2} + P_H - P = 0 \ . \tag{A.8}$$

From Eq. (A.1), the equilibrium relations may be written as

$$P_{CO} = K_1 \frac{P_{CO_2}}{\sqrt{P_{O_2}}} \qquad P_{H_2O} = \frac{P_{H_2}}{K_2} \sqrt{P_{O_2}} \qquad P_{OH} = \frac{K_3}{K_2} \sqrt{P_{H_2} P_{O_2}}$$

$$P_H = K_4 \sqrt{P_{H_2}} \quad \text{and} \quad P_O = K_5 \sqrt{P_{O_2}} \ , \tag{A.9}$$

where K is the equilibrium constant defined as

$$K = \exp\left[\frac{-\sum_{j}^{n}(\beta_j - \alpha_j)\mu_j^{o}}{\hat{R}T}\right] , \qquad (A.10)$$

where the chemical potentials, μ^o (or Gibbs free energy per mole), are as given by [20].

Since Eq. (A.9) can be arranged such that p_O, p_{OH}, p_{CO}, p_H, and p_{H_2O} are explicit functions of p_{H_2}, p_{O_2}, and p_{CO_2}, they may be substituted into Eqs. (A.6) to (A.8). This gives three equations for the three unknowns, p_{H_2}, p_{O_2}, and p_{CO_2}.

A Newton-Raphson procedure is then applied which converges very rapidly. That is, Eqs. (A.6) to (A.8) are linearized [32] as

$$\delta F = \frac{\partial F}{\partial p_{H_2}}\delta p_{H_2} + \frac{\partial F}{\partial p_{O_2}}\delta p_{O_2} + \frac{\partial F}{\partial p_{CO_2}}\delta p_{CO_2} ,$$

$$\delta G = \frac{\partial G}{\partial p_{H_2}}\delta p_{H_2} + \frac{\partial G}{\partial p_{O_2}}\delta p_{O_2} + \frac{\partial G}{\partial p_{CO_2}}\delta p_{CO_2} , \qquad (A.11)$$

$$\delta L = \frac{\partial L}{\partial p_{H_2}}\delta p_{H_2} + \frac{\partial L}{\partial p_{O_2}}\delta p_{O_2} + \frac{\partial L}{\partial p_{CO_2}}\delta p_{CO_2} .$$

A first guess of p_{H_2}, p_{O_2}, and p_{CO_2} gives the initial residuals, F, G, and L, and also the values of the partial derivatives. These three equations (Eq. (A.11)) are linear equations for δp_{H_2}, δp_{O_2}, and δp_{CO_2} with the new F, G, and L being set to zero; that is,

$$\delta F = -F \ ,$$

$$\delta G = -G \ , \qquad \text{(A.12)}$$

$$\delta L = -L \ .$$

The new guesses of the unknowns are then

$$p_{new} - p_{initial} = \delta p \ . \qquad \text{(A.13)}$$

The new partial pressures become the first guesses, and the procedure is continued until the residuals are satisfactorily small.

APPENDIX B

A SUGGESTED RESOLUTION OF THE PROBLEM OF THE PROFILE SHIFT WHEN CONSIDERING AXIALLY SYMMETRIC MIXING

In the following, a method is suggested for determining y_m and C_{mf} for axially symmetric mixing. That calculations based on this approach are not presented is because the approach was not apparent until late in the life of the project. However, it will be used as a basis for further refinement of the theory to be taken up at a later date.

Equations (17) and (18) of the two-dimensional theory are repeated here as

$$\left[\int_0^{y_U} \rho_s u_s \, dy\right]_{x=0} = \left[\int_{y_L}^{y_U+y_m} k\rho u \, dy\right]_{x=\ell} \tag{B.1}$$

and

$$\left[\int_0^{y_U} \rho_s u_s^2 \, dy\right]_{x=0} = \left[\int_{y_L}^{y_U+y_m} \rho u^2 dy\right]_{x=\ell} , \tag{B.2}$$

with

$$k = \frac{1}{2}\left[1 + \operatorname{erf}\left(C_{mf}\eta\right)\right] . \tag{B.3}$$

For two-dimensional mixing, Eqs. (B.1) and (B.2) are sufficient for determining both C_{mf} and y_m.

In words, these equations say that when the mixing profile is localized such that y_m is the distance from the origin to the inviscid boundary, at $x = \ell$, then the mass and momentum of the initial profile out to the streamline, y_U, are preserved. The streamline, y_U, is determined at $x = \ell$ such that $\phi = 0.99998895$. In two-dimensional flow, the streamline, y_U, can be traced, parallel to the inviscid boundary, to the beginning of mixing. With axially symmetric mixing, y_U is not parallel to the inviscid boundary. At this point, for axially symmetric mixing, there is not enough information to solve the problem.

It is important, also, at this point to stress certain elements of the theory.

1. The boundary layer is considered as part of the inviscid flow; that is, the boundary layer is an inviscid, rotational profile and no more.
2. Equations (B.1) and (B.2) are actually relations between the inviscid flow, the left-hand side, and the viscous mixing, the right-hand side.

With this in mind, Eqs. (B.1) and (B.2) for two-dimensional mixing may also be formulated as

$$\left[\int_{y_m}^{y_m+y_U} \rho_s u_s \, dy\right]_{x=\ell} = \left[\int_{y_L}^{y_U+y_m} k\rho u \, dy\right]_{x=\ell} \tag{B.4}$$

and

$$\int_{y_m}^{y_m+y_U} \rho_s u_s^2 dy \Big]_{x=\ell} = \int_{y_L}^{y_U+y_m} \rho u^2 dy \Big]_{x=\ell} . \tag{B.5}$$

That these relations are equivalent to Eqs. (B.1) and (B.2) requires only the observation that an inviscid profile in two-dimensional flow, subject to no pressure gradients or dissipative mechanisms, remains intact. In other words, Eqs. (B.4) and (B.5) say that, locally, the mass and momentum rates of the viscous layer are equal to the mass and momentum rates of the inviscid field from its boundary to the same y location, at the same x station.

With these observations in mind, the axially symmetric equivalent of Eqs. (B.4) and (B.5) may be formulated as

$$2\pi \int_{y_m}^{y_m+y_U} (\rho u)^* R dy \Big]_{x=\ell} = 2\pi \int_{y_L}^{y_U+y_m} k\rho u R dy \Big]_{x=\ell} \tag{B.6}$$

and

$$2\pi \int_{y_m}^{y_m+y_U} (\rho u^2)^* R dy \Big]_{x=\ell} = 2\pi \int_{y_L}^{y_U+y_m} \rho u^2 R dy \Big]_{x=\ell} . \tag{B.7}$$

The asterisk used above and in the following serves to keep track of the fact that in the axially symmetric case, the boundary layer thickness and shape are not the same at $x = \ell$ as they are at $x = o$. That is, now the

problem is complicated by the fact that if

$$u_s/U = (y/\delta)^{\frac{1}{n}} \tag{B.8}$$

is the initial velocity profile, at x = ℓ

$$u/U = (y/\delta^*)^{\frac{1}{n^*}} , \tag{B.9}$$

where

$$\delta^* \neq \delta \tag{B.10}$$

and

$$n^* \neq n \ . \tag{B.11}$$

The parameters, δ^* and n^*, may be found as follows. Consider that the following relations hold for the inviscid flow at constant pressure and with no dissipative mechanisms.

$$2\pi \int_o^{\delta} \rho_s U (y/\delta)^{1/n} \, Rdy \Big]_{x=o} = 2\pi \int_{y_m}^{y_m+\delta^*} \rho U (y/\delta^*)^{1/n^*} \, Rdy \Big]_{x=\ell} \tag{B.12}$$

and

$$2\pi \int_o^{\delta} \rho_s U^2 (y/\delta)^{2/n} \, Rdy \Big]_{x=o} = 2\pi \int_{y_m}^{y_m+\delta^*} \rho U^2 (y/\delta^*)^{2/n^*} \, Rdy \Big]_{x=\ell} \ . \tag{B.13}$$

Thus, there now exist sufficient relations to solve the axially symmetric problem. The four relations, then, Eqs. (B.6), (B.7), (B.12), and (B.13) along with Eq. (B.3) serve to determine the four unknowns, δ^*, n^*, C_{mf}, and y_m.

It is realized, of course, that as these computations will be embedded in the overall base-pressure iteration, they further degrade the efficiency of the global calculations.

APPENDIX C

DEVELOPMENT OF THE CHARACTERISTIC AND COMPATIBILITY EQUATIONS

Consider the conservation equations for mass, z and r, momentum and energy as

$$\rho v + r \frac{\partial \rho v}{\partial r} + r \frac{\partial \rho u}{\partial z} = 0 \ , \tag{C.1}$$

$$\rho u \frac{\partial u}{\partial z} + \rho v \frac{\partial u}{\partial r} + \frac{\partial p}{\partial z} = 0 \ , \tag{C.2}$$

$$\rho u \frac{\partial v}{\partial z} + \rho v \frac{\partial v}{\partial r} + \frac{\partial p}{\partial r} = 0 \ , \tag{C.3}$$

$$\rho u \frac{\partial H}{\partial z} + \rho v \frac{\partial H}{\partial r} = 0 \ , \tag{C.4}$$

with

$$H = \frac{1}{2} (u^2 + v^2) + h \tag{C.5}$$

and

$$\rho = f (p, h) \ . \tag{C.6}$$

These constitute the set of equations for u, v, p, and h. Now, using

$$\frac{\partial \rho}{\partial z} \Big)_r = \frac{\partial \rho}{\partial p} \frac{\partial p}{\partial z} + \frac{\partial \rho}{\partial h} \frac{\partial h}{\partial z} \tag{C.7}$$

and

$$\frac{\partial \rho}{\partial r} \Big)_z = \frac{\partial \rho}{\partial p} \frac{\partial p}{\partial r} + \frac{\partial \rho}{\partial h} \frac{\partial h}{\partial r} \ , \tag{C.8}$$

Eqs. (C.1) through (C.4) may be cast in the form

$$A \frac{\partial \vec{W}}{\partial z} + B \frac{\partial \vec{W}}{\partial r} + \vec{C} = 0 , \qquad (C.9)$$

where

$$A = \begin{bmatrix} \rho & 0 & u \frac{\partial \rho}{\partial p} & u \frac{\partial \rho}{\partial h} \\ \rho u & 0 & 1 & 0 \\ 0 & \rho u & 0 & 0 \\ \rho u^2 & \rho uv & 0 & \rho u \end{bmatrix} , \qquad (C.10)$$

$$B = \begin{bmatrix} 0 & \rho & v \frac{\partial \rho}{\partial p} & v \frac{\partial \rho}{\partial h} \\ \rho v & 0 & 0 & 0 \\ 0 & \rho v & 1 & 0 \\ \rho uv & \rho v^2 & 0 & \rho v \end{bmatrix} , \qquad (C.11)$$

$$\vec{C} = \begin{bmatrix} \frac{\rho v}{r} \\ 0 \\ 0 \\ 0 \end{bmatrix} , \qquad (C.12)$$

and

$$\vec{W} = \begin{bmatrix} u \\ v \\ p \\ h \end{bmatrix} . \qquad (C.13)$$

It is desired to find curves in the region of interest along which the set of partial differential equations reduce to ordinary differential equations. Consider the definition of a total differential

$$d\vec{W} = \frac{\partial \vec{W}}{\partial z} dz + \frac{\partial \vec{W}}{\partial r} dr . \qquad (C.14)$$

Along a given curve, dr and dz are no longer independent, so that

$$\frac{d\vec{W}}{dz} = \frac{\partial \vec{W}}{\partial z} + \frac{\partial \vec{W}}{\partial r} \frac{dr}{\partial z} . \qquad (C.15)$$

Using Eq. (C.15) to eliminate $\frac{\partial \vec{W}}{\partial z}$,

$$A \left(\frac{d\vec{W}}{dz} - \frac{\partial \vec{W}}{\partial r} \frac{dr}{dz} \right) + B \frac{\partial \vec{W}}{\partial r} + \vec{C} = 0 \qquad (C.16)$$

is obtained.

Taking the remaining partial derivative to the right-hand side gives

$$A \frac{d\vec{W}}{dz} + \vec{C} = \left(\frac{dr}{dz} A - B \right) \frac{\partial \vec{W}}{\partial r} . \qquad (C.17)$$

Now, it is observed that if a vector were found that was orthogonal to the vectors of Eq. (C.17) and the inner product were taken, Eq. (C.17) would appear as

$$\left(A \frac{d\vec{W}}{dz} + \vec{C} \right) \cdot \vec{\Lambda} = 0 \ , \qquad (C.18)$$

which is the form that is sought; that is, Eq. (C.18) is an ordinary differential equation. Thus, associated with each $\frac{dr}{dz}$, a vector is found such that

$$\left(A \frac{dr}{dz} - B \right) \frac{\partial \vec{W}}{\partial r} \cdot \vec{\Lambda} = 0 \ . \qquad (C.19)$$

To solve for such a vector, a property of the scalar product is used to put Eq. (C.19) in the form

$$\frac{\partial \vec{W}}{\partial r} \cdot \left(\frac{dr}{dz} - B \right)^T \vec{\Lambda} = 0 \ , \qquad (C.20)$$

where the superscript, T, means transpose. Now, since $\frac{\partial \vec{W}}{\partial r}$ is assumed to be nonzero, it is sufficient that

$$\left(A \frac{dr}{dz} - B \right)^T \vec{\Lambda} = \vec{\Theta} \ , \qquad (C.21)$$

where $\vec{\Theta}$ is the null vector.

From linear algebra, for there to exist nontrivial solutions to a homogeneous set of equations, the determinant of the coefficient matrix must be zero. Thus,

$$\text{Det} \left| A \frac{dr}{dz} - B \right|^T = 0 \ . \qquad (C.22)$$

This condition forces specific conditions on $\frac{dr}{dz}$ as it is a polynomial in $\frac{dr}{dz}$. These are called the characteristic equations. For this case, they are

$$\left(\frac{dr}{dz}\right)_1 = \left(\frac{dr}{dz}\right)_2 = \frac{v}{u} \quad , \tag{C.23}$$

$$\left(\frac{dr}{dz}\right)_3 = \frac{uv + a\sqrt{u^2 + v^2 - a^2}}{u^2 - a^2} \quad , \tag{C.24}$$

and

$$\left(\frac{dr}{dz}\right)_4 = \frac{uv - a\sqrt{u^2 + v^2 - a^2}}{u^2 - a^2} \quad . \tag{C.25}$$

These $\frac{dr}{dz}$ relations are substituted one at a time back into the homogeneous set (Eq. (C.21)), and the components of four different vectors are found corresponding to each $\frac{dr}{dz}$.

For the case at hand, these four vectors associated with the corresponding $\frac{dr}{dz}$ just determined are

$$\vec{\Lambda}_1 = \begin{bmatrix} 0 \\ 1 \\ \frac{v}{u} \\ 0 \end{bmatrix} \qquad \vec{\Lambda}_2 = \begin{bmatrix} 0 \\ 0 \\ 0 \\ 1 \end{bmatrix} \tag{C.26}$$

---

[1] Because of the choice of dependent variables

$$a^2 = \rho / \left(\frac{\partial \rho}{\partial h} + \rho \frac{\partial \rho}{\partial p}\right) .$$

and

$$\Lambda_{3,4} = \begin{bmatrix} \rho \left[u \left(\frac{dr}{dz} \right)_{3,4} - v \right] \\ \left[u \left(\frac{dr}{dz} \right)_{3,4} - v \right] u \frac{\partial \rho}{\partial h} - \rho \left(\frac{dr}{dz} \right)_{3,4} \\ \rho + \left[u \left(\frac{dr}{dz} \right)_{3,4} - v \right] v \frac{\partial \rho}{\partial h} \\ - \left[u \left(\frac{dr}{dz} \right)_{3,4} - v \right] \frac{\partial \rho}{\partial h} \end{bmatrix} , \qquad (C.27)$$

where the last two vectors satisfy Eq. set (C.21) when Eqs. (C.24) and (C.25) are substituted for $\frac{dr}{dz}$.

Now, having these four vectors, the ordinary differential equations associated with each $\frac{dr}{dz}$ are found by substituting each vector into Eq. (C.18) and performing the inner product. The differential equation found for each vector is called the compatibility relation valid along the associated curve described by the particular $\frac{dr}{dz}$. For $\vec{\Lambda}_1$,

$$udu + udv + \frac{dp}{\rho} = 0 \ . \qquad (C.28)$$

For $\vec{\Lambda}_2$,

$$dh + udu + vdv = 0 \ , \qquad (C.29)$$

and for $\vec{\Lambda}_{3,4}$,

$$\left[u\left(\frac{dr}{dz}\right)_{3,4} - v\right]\left[udv - vdu\right] + \frac{vdz}{r}\left[u^2\left(\frac{dr}{dz}\right)^2_{3,4} - uv\left(\frac{dr}{dz}\right)_{3,4} + v^2\right]$$

$$+ \frac{dp}{\rho}\left[v\left(\frac{dr}{dz}\right)_{3,4} + u\right] = 0 \ . \qquad (C.30)$$

Thus, the four ordinary differential equations for the four curves defined by the $\frac{dr}{dz}$'s are found.

LIST OF SYMBOLS

Where a symbol is defined only for the purpose of discussion within the text, it may not be listed here. Chemical elements are not listed because of their universality.

a	Local frozen speed of sound
c_p	Specific heat at constant pressure
C	Mole fraction of molecular species
C_{mf}	Shape parameter of mass fraction distribution
E	Base-bleed parameter, Fig. 14
h	Enthalpy
h	One-half of the height of the base in axially symmetric flows; i.e., $(R_2 - R_1)/2$; the base height in planar backstep flows
H	Total enthalpy
k	In the mixing layer, the mass fraction of the high-speed stream in the local mixture, Eq. (16)
$\bar{k}$	A mixing-length constant, Eq. (40)
K	Equilibrium gas constant, Eq. (A.11)
ℓ	A specific x-location in the mixing layer
$\bar{\ell}$	Prandtl's mixing length
m	Number of atoms present
$\dot{m}$	Rate of mass flow
M	Mach number
n	Number of species present

N	Mole-atoms per unit mass of mixture
p	Pressure
p_r	Recovered pressure, after recompression process
P	Total pressure
P	Fictitious partial pressure of atom
r	Transverse coordinate in method of characteristics
R	Radius from axis of symmetry to point in mixing layer
R	Gas constant of molecular species
$\hat{R}$	Universal gas constant
Re_θ	Reynolds number based on momentum thickness
s	Entropy
t	Temperature
T	Total temperature
u	Velocity component in direction of developing mixing layer
u	Axial component of velocity in method of characteristics
v	Transverse velocity component
w	Molecular weight
x	Mixing-layer coordinate in the direction of development
X	Coordinate along recompression on slipline
y	Transverse mixing-layer coordinate
z	Axial coordinate in method of characteristics
α_j	Number of moles of species j (reactants)

β_j	Number of moles of species j (products)
β	Angle of inviscid boundary with undisturbed free stream
γ	Isentropic exponent
γ	Relative angle of inviscid boundary with slipline at intersection point of inviscid boundaries
δ	Boundary-layer thickness
δ^*	Boundary-layer displacement thickness
ϵ	Apparent kinematic viscosity
ζ	Transformed coordinate of Eq. (9), $\int_0^x \epsilon_o F(x)/U dx$
η	Dimensionless mixing variable, $\sigma y/x$
η_p	Dimensionless position parameter, $\sigma\delta/x$
θ	Boundary-layer momentum thickness
μ^o	Gibbs free energy per mole
ρ	Density
σ	Mixing or spreading parameter
σ_o	Incompressible σ, a reference value
ϕ	Velocity ratio, u/U
ω	Angle between slipline and axial direction

Subscripts

A	Axially symmetric value
B	Base region
D	Dividing streamline
E	Bleed
i	ith species
i	Intersection point of inviscid boundaries

J	Jet
L	Quiescent or base edge of mixing layer
m	Regarding inviscid boundary and coordinate increment defined in Eq. (15)
s	At point of separation, initiation of mixing
S	Stagnating streamline
S1	Stream 1, Fig. 1
S2	Stream 2, Fig. 1
U	High-speed edge of mixing layer
∞	At undisturbed free-stream conditions
1	Beginning of recompression
1	Of Stream 1, Fig. 1
2	End of recompression
2	Of Stream 2, Fig. 1